EurJIC
European Journal of Inorganic Chemistry

Full Paper
doi.org/10.1002/ejic.202000800

Supported Silyl Cations

Silyl Cations Stabilized by Pincer Type Ligands with Adjustable Donor Atoms

Andreas Denhof,[a] Marian Olaru,[a,d] Enno Lork,[a] Stefan Mebs,[b] Lilianna Chęcińska,*[a,c] and Jens Beckmann*[a]

Dedicated to Professor Klaus Jurkschat on the occasion of his retirement from the Technical University of Dortmund.

Abstract: Novel E,C,E′-pincer supported silyl cations (E, E′ = O, S, Se, Au) were prepared in three steps starting from 2,6-$F_2C_6H_3SiMe_2H$ (**1a**) and 2,6-$Br_2C_6H_3SiMe_2H$ (**1b**), which were first converted in two complementary ways into 2,6-$(Ph_2P)_2C_6H_3SiMe_2H$ (**2**). The oxidation of **2** with H_2O_2·urea, S_8, and Se_8 afforded 2,6-$(Ph_2PE)_2C_6H_3SiMe_2H$ (**3a**, E = O; **3b**, E = S; **3c**, E = Se) and 2-(Ph_2PE)-6-(Ph_2P)-$C_6H_3SiMe_2H$ (**4b**, E = S; **4c**, E = Se), which were reacted to the E,C,E-supported silyl cations $[2,6\text{-}(Ph_2PE)_2C_6H_3SiMe_2]^+$ (**5a**, E = O, counterion Br_3^-; **5b**, E = S, counterion $B(C_6F_5)_4^-$; **5c**, E = Se, counterion $B(C_6F_5)_4^-$), the E,C-supported silyl cations $[2\text{-}(Ph_2PE)\text{-}6\text{-}(Ph_2P)C_6H_3SiMe_2]^+$ (**6b**, E = S, not isolated; **6c**, E = Se, not isolated), the O,C,S-supported silyl cation $[2\text{-}(Ph_2PS)\text{-}6\text{-}(Ph_2PO)C_6H_3SiMe_2]^+$ (**7**, counterion $B(C_6F_5)_4^-$) as well as the E,C,Au-supported silyl cations $[2\text{-}(Ph_2PAuC_6F_5)\text{-}6\text{-}(Ph_2PE)C_6H_3SiMe_2]^+$ (**8b**, E = S, counterion $[B\{3,5\text{-}(CF_3)_2C_6H_3\}_4]^-$; **8c**, E = Se, $[B\{3,5\text{-}(CF_3)_2C_6H_3\}_4]^-$) using Br_2, O_2, S_8, (tht)AuC_6F_5, $Ph_3C[B(C_6F_5)_4]$ and $Ph_3C[B\{3,5\text{-}(CF_3)_2C_6H_3\}_4]$. All compounds were characterized by multinuclear (^1H, ^{13}C, ^{19}F, ^{29}Si, ^{31}P, ^{77}Se) NMR spectroscopy, ESI MS spectrometry and X-ray crystallography (**2**, **3a**·H_2O, **3b**, **3c**, **4b**, **5a**, **5c**, **7**, **8b**, **8c**). The gas phase structures of **2**, **3a–c**, **5a–c** (fully optimized) and **8b**, **8c** (single-point calculations) were studied at the B3PW91/6-311+G(2df,p) level of theory. A set of real-space bonding indicators (RSBIs) derived from the theoretically calculated electron and pair densities were analyzed utilizing the atoms-in molecules (AIM) and electron-localizability indicator (ELI-D) space partitioning schemes.

Introduction

The isolation of tricoordinate silyl cations posed an exceptional challenge for several decades.[1] So far only two genuinely tricoordinate silyl cations $[R_3Si]^+[A]^-$ (**I**), namely $[Mes_3Si]^+[HCB_{11}Me_5Br_6]^-$,[2] and $[Pemp_3Si]_2^+[B_{12}Cl_{12}]^{2-}$[3] have successfully been prepared by the judicious choice of bulky and electron rich substituents and weakly coordinating anions (Mes = mesityl; Pemp = pentamethylphenyl). The difficult preparation can arguably be attributed to the extreme Lewis acidity of tricoordinate silyl cations and their high reactivity towards almost all σ and π-donors, including many counterions and solvent molecules.[1] The presence of coordinating anions (A^-) and neutral donors (D) inevitably increases the coordination number of the silicon atoms from CN = 3 in $[R_3Si]^+[A]^-$ (**I**) to CN = 3 + 1 in $[R_3Si^+\cdots A^-]$ (**II**) and $[(R_3Si\cdots D)]^+[A]^-$ (**IV**) or even CN = 3 + 2 in $[R_3Si^+\cdots(A^-)_2]$ (**III**) and $[(R_3Si\cdots D_2)]^+[A]^-$ (**V**), respectively, and dramatically reduces the Lewis acidity (Scheme 1).[1] The prerequisite of kinetically stabilizing bulky substituents *and* weakly coordinating anions for the stabilization of tricoordinate silyl cations $[R_3Si]^+[A]^-$ (**I**) can be nicely deduced by inspection of a series of published compounds. In the absence of bulky substituents, contact ion pairs $[R_3Si^+\cdots A^-]$ (**II**) were obtained as illustrated in $[Me_3Si^+\cdots RCB_{11}F_{11}^-]$ (R = H, Me),[4] $[(R_3Si^+)_2\cdots B_{12}Cl_{12}^{2-}]$ (R = Me, Et, *i*Pr),[5] and $[Et_3Si^+\cdots HCB_{11}H_5Cl_6^-]$[6] although weakly coordinating borane or carborane anions have been employed. The recently reported $[H_3Si^+\cdots HCB_{11}H_5Br_6^-]$ is a straightforward example of the type $[R_3Si^+\cdots(A^-)_2]$ (**III**) in which the substituted carborane anions bridged between the parent H_3Si^+ (Scheme 1).[7]

[a] *Dr. A. Denhof, Dr. M. Olaru, Dr. E. Lork, Dr. L. Chęcińska, Prof. Dr. J. Beckmann*
Institut für Anorganische Chemie und Kristallographie, Universität Bremen, Leobener Straße 7, 28359 Bremen, Germany
E-mail: Lilianna.checinska@chemia.uni.lodz.pl
j.beckmann@uni-bremen.de
https://www.uni-bremen.de/beckmann/
[b] *Dr. S. Mebs*
Institut für Experimentalphysik, Freie Universität Berlin, Arnimallee 14, 14195 Berlin, Germany
[c] *Dr. L. Chęcińska*
Department of Theoretical and Structural Chemistry, Faculty of Chemistry, University of Lodz, Pomorska 163/165, 90-236 Lodz, Poland
[d] *Dr. M. Olaru*
Department of Chemistry, Supramolecular Organic and Organometallic Chemistry Centre Babes-Bolyai University, 11 Arany Janos, 400028 Cluj-Napoca, Romania
Supporting information and ORCID(s) from the author(s) for this article are available on the WWW under https://doi.org/10.1002/ejic.202000800.

This manuscript is part of the Special Collection Pincer Chemistry and Catalysis.

Full Paper
doi.org/10.1002/ejic.202000800

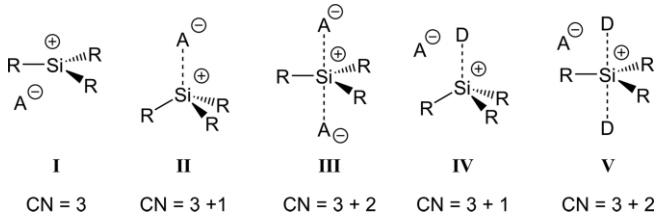

Scheme 1. Spatial arrangement of silyl cations **I**–**IV** with different coordination numbers (CN).

In the presence of (substituted) benzene (derivatives), Lewis pair complexes $[(R_3Si\cdots D)]^+[A]^-$ (**IV**) such as $[(Me_3Si\cdots arene)]^+[B(C_6F_5)_4]^-$ were isolated in which the arenes serve as π-donors (arene = benzene, toluene etc.).[8] Some of these species may be even viewed as silyl-substituted arenium ions. The use of one bulky *m*-terphenyl substituent (occasionally decorated by halogen atoms at the flanking phenyl groups) gave rise to the formation of intramolecularly coordinated donor acceptor complexes, such as $[(2,6\text{-}Mes_2C_6H_4)Me_2Si]^+[B(C_6F_5)_4]^-$.[9] In the ferrocenyl-substituted silyl cation $[FcMe_2Si]^+_2[B_{12}Cl_{12}]^{2-}$, the iron intramolecularly provides electron density to the electron deficient silicon atom (Fc = ferrocenyl).[10]

The vast majority of silyl cations have been prepared by a variation of the Bartlett–Condon–Schneider reaction using trityl salts of weakly coordinating anions $[Ph_3C]^+[A]^-$ for the hydride abstraction from neutral H-silanes R_3SiH. Quite often, these reactions produced hydride-bridged silyl cations $[R_3Si(\mu\text{-}H)SiR_3]^+$ possessing three-center two electron (3c2e) bonds, rather than "free" silyl cations.[11] Despite having a somewhat reduced Lewis acidities some of the higher-coordinated silyl cations show remarkable catalytic activities,[12] including C–F bond activation/hydrodefluorination reactions[6,13] and Diels-Alder reactions.[14] The combination of silyl cations and bulky phosphanes has been considered as frustrated Lewis pairs (FLPs) for the fixation and activation of carbon dioxide and dihydrogen.[15]

Pentacoordinate silyl cations $[(R_3Si\cdots D_2)]^+[A]^-$ (**V**) have also been prepared deliberately using intramolecularly coordinating substituents with donor atoms (so-called built in ligands).[16] A prominent and significant example involves the O,C,O-pincer supported silyl cation $[4\text{-}t\text{Bu-}2,6\text{-}\{(i\text{PrO})_2P(O)\}_2C_6H_3(Ph_2)Si]^+$ (**VI**, counterion PF_6^-) containing two intramolecularly coordinating phosphonium oxide groups (Scheme 2).[17]

It is nowadays understood that phosphonium oxides are best described by bipolar single bonds +P–O⁻ rather than P=O double bonds.[18] At present, there is a vivid debate how to present donor acceptor interactions within main group complexes and it has been pleaded to avoid extreme resonance formulas for marketing reasons.[19] In the centre of this debate are often low-coordinate cations, which are stabilized by phosphine ligands or N-heterocyclic carbenes (NHCs). Although this work is not concerned with these compound classes, the question for the most significant resonance structure for the description of silyl cations, such as **VI**, also requires clarification and will be discussed below. Like the tricoordinate silyl cations $[Mes_3Si]^+[HCB_{11}Me_5Br_6]^-$,[2] and $[Pemp_3Si]^+_2[B_{12}Cl_{12}]^{2-}$,[3] **VI** possesses a trigonal planar base consisting of three C atoms.[17] In addition to the tricoordinate silyl cations **V** comprises two axial

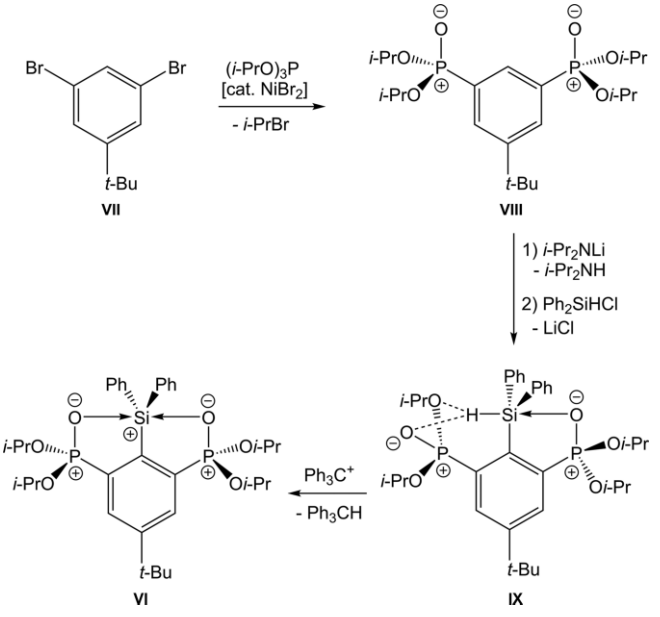

Scheme 2. Synthetic route for the preparation of Jurkschat's O,C,O-pincer supported silyl cation **VI**.[17]

O atoms that compensate the electron deficiency of the Si atom. For both tricoordinate silyl cations $[R_3Si^+][A^-]$ (**I**) and pentacoordinate silyl cations $[(R_3Si\cdots D_2)]^+[A]^-$ (**V**), a simplistic "valence bond (VB) model" might attribute the bonding of the three equatorial substituents to three sp^2-orbitals. It might further describe the axial substituents D of the pentacoordinate silyl cations $[(R_3Si\cdots D_2)]^+[A]^-$ (**V**) as three-center four electron (3c4e) bonds involving the p_z-orbital of the Si atom.[16] In the tricoordinate silyl cations $[R_3Si]^+[A]^-$ (**I**) the p_z-orbital remains vacant. Most recent computational work attributes the high affinity of Si for O to the high electronegativity differences and emphasizes the strongly polar or even ionic bond character of the Si–O bond,[20] which questions strong covalent contributions for the axial bonding in pentacoordinate silyl cations such as **V**. We became interested in the preparation of new E,C,E′-pincer supported silyl cations with a number of different donor atoms E, E′ = O, S, Se, Au including also those with a smaller affinity and electronegativity difference between Si and O. The established synthetic route for the preparation of the O,C,O-pincer supported silyl cation **VI** starts from the dibromo benzene **VII**, which was converted into the diphosphonate **VIII** by a transition metal catalyzed Arbuzov reaction, which restricts the donor atoms of this pincer ligand to O atoms.[17] We note in passing that efforts were undertaken to prepare related O,C,S-pincer ligands, which, however, rely on the Arbuzov reaction.[21] The selective C–H metallation of **VIII** prior to the reaction with Ph_2SiHCl gives rise to the formation of the H-silane **IX**. Hydride abstraction from **IX** via the Bartlett–Condon–Schneider reaction eventually provided the silyl cation **VI**.[17] In this work we present an alternative route that first introduces the Si moiety and avoids Arbuzov type reactions, which allows setting up more versatile pincer type ligands.[22] Using this route, a number of new E,C,E′-pincer supported silyl cations with various potential donor atoms (E, E′ = O, S, Se, Au) have been prepared

and fully characterized. The nature of the bonds within these compounds was determined by analysis of a set of topological and integrated real-space bonding indicators (RSBIs) derived from the theoretically calculated electron densities (ED) and electron pair densities utilizing the atoms-in-molecules (AIM)[23] and electron-localizability-indicator (ELI-D)[24] space partitioning schemes which divide space in basins of atoms and paired electrons, respectively. A combination of these two methods provides quantitative information about the strength and nature of a bond and is very well suited to straightforwardly detect also weak atomic interactions, which is not the case for sole inspection of molecular orbitals (MOs) and/or natural bond orbitals (NBOs).

Results and Discussion

Synthetic Aspects

2,6-Difluorodimethylsilylbenzene, 2,6-$F_2C_6H_3SiMe_2H$ (**1a**), was prepared by the reaction of 2,6-difluorophenyllithium, 2,6-$F_2C_6H_3Li$,[25] with $HSiMe_2Cl$, adapting a literature procedure published for 2,6-$F_2C_6H_3SiMe_3$.[26] 2,6-Dibromodimethylsilylbenzene, 2,6-$Br_2C_6H_3SiMe_2H$ (**1b**), was obtained similarly as already described.[27] The preparation of 2,6-bis(diphenylphosphino)-dimethylsilylbenzene, 2,6-$(Ph_2P)_2C_6H_3SiMe_2H$ (**2**), was achieved in two complementary ways, namely, the reaction of **1a** with two equivalents of Ph_2PLi and the double lithiation of **1b** with *n*BuLi/TMEDA prior to the reaction with two equivalents of Ph_2PCl, respectively (Scheme 3). The former reaction entails a nucleophilic substitution at the aromatic ring, while the latter involves a nucleophilic substitution at the P atom. The oxidation of **2** with a slight excess of H_2O_2·urea, S_8 and Se_8 provided the 2,6-bis(diphenylphosphinchalcogenido)dimethylsilylbenzenes 2,6-$(Ph_2PE)_2C_6H_3SiMe_2H$ (**3a**, E = O; **3b**, E = S; **3c**, E = Se).

The reaction of **2** with one equivalent of S_8 and Se_8 gave 2-(diphenylphosphinchalcogenido)-6-(diphenylphosphino)dimethylsilylbenzene, 2-(Ph_2PE)-6-(Ph_2P)-$C_6H_3SiMe_2H$ (**4b**, E = S; **4c**, E = Se), in good selectivity (Scheme 3). The precursors **2–4** were purified by crystallization and obtained as air-stable crystalline materials. The preparation of the O,C,O-pincer supported silyl cation $[2,6\text{-}(Ph_2PO)_2C_6H_3SiMe_2]^+$ (**5a**; counterion Br_3^-) was achieved by the simple oxidation of 2,6-$(Ph_2PO)_2C_6H_3SiMe_2H$ (**3a**) with an excess bromine (Scheme 4). Attempts to prepare the same O,C,O-pincer supported silyl cation **5a** by the established Bartlett–Condon–Schneider reaction using $[Ph_3C^+][B(C_6F_5)_4]$ proved unsuccessful and afforded an unaccounted mixture of products. In one experiment a small crop of $Ph_3COOCPh_3$ was isolated, however, it is unclear if it is related to the preferred reaction, or simply a side-product formed by traces of molecular oxygen (see ESI for details).

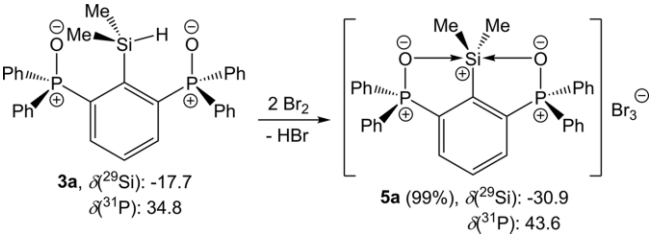

Scheme 4. Formation and selected NMR data of the O,C,O- supported silyl cation **5a**.

The Bartlett–Condon–Schneider reaction of the heavier analogs **3b** and **3c** afforded in each case two organometallic products. The product distribution was inferred by integration of the

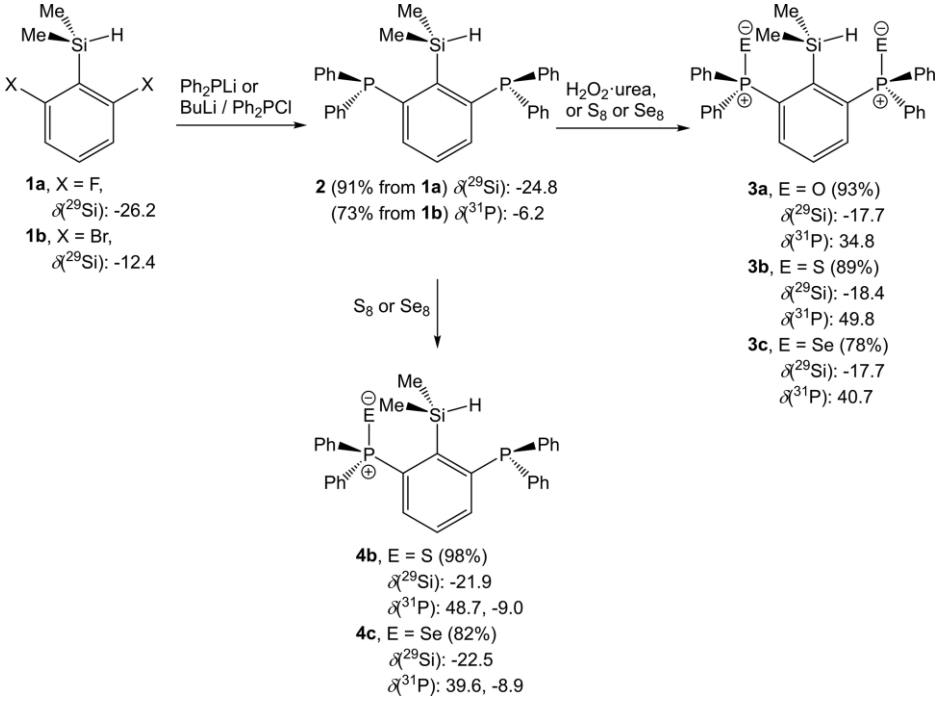

Scheme 3. Formation and selected NMR data of the precursors **2–4**.

Full Paper
doi.org/10.1002/ejic.202000800

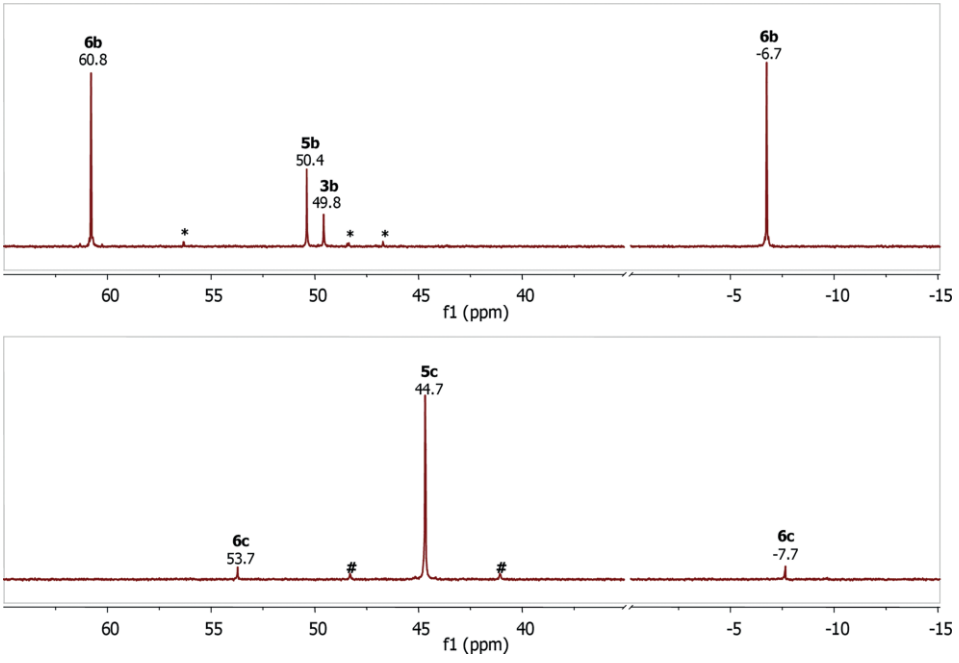

Figure 1. ^{31}P NMR spectrum of the Bartlett–Condon–Schneider reaction of **3b** (top) and **3c** (bottom) with $[Ph_3C][B(C_6F_5)_4]$ (unassigned products and ^{77}Se satellites are marked by asterisks and hashtags, respectively).

^{31}P NMR resonances. The ^{31}P NMR spectra of the crude reaction mixtures are shown in Figure 1.

The reaction of 2,6-$(Ph_2PS)_2C_6H_3SiMe_2H$ (**3b**) and $[Ph_3C][B(C_6F_5)_4]$ gave a mixture of the desired S,C,S-supported silyl cation $[2,6\text{-}(Ph_2PS)_2C_6H_3SiMe_2]^+$ (**5b**, 10 %), the unexpected S,C-supported silyl cation $[2\text{-}(Ph_2PS)\text{-}6\text{-}(Ph_2P)C_6H_3SiMe_2]^+$ (**6b**, 74 %), and the starting material **3b** (9 %) that was not separated (Scheme 5). The side-product of the formation of **6b**, tritylthiol Ph_3CSH was isolated from the mother liquor by column chromatography and unambiguously identified by comparison with an authentic sample. The reaction of 2,6-$(Ph_2PSe)_2C_6H_3SiMe_2H$ (**3c**) and $[Ph_3C][B(C_6F_5)_4]$ gave a mixture of the desired Se,C,Se-supported silyl cation $[2,6\text{-}(Ph_2PSe)_2C_6H_3SiMe_2]^+$ (**5c**, 90 %) and the unexpected Se,C-supported silyl cation $[2\text{-}(Ph_2PSe)\text{-}6\text{-}(Ph_2P)C_6H_3SiMe_2]^+$ (**6c**, 10 %) from which the former was isolated (Scheme 5).

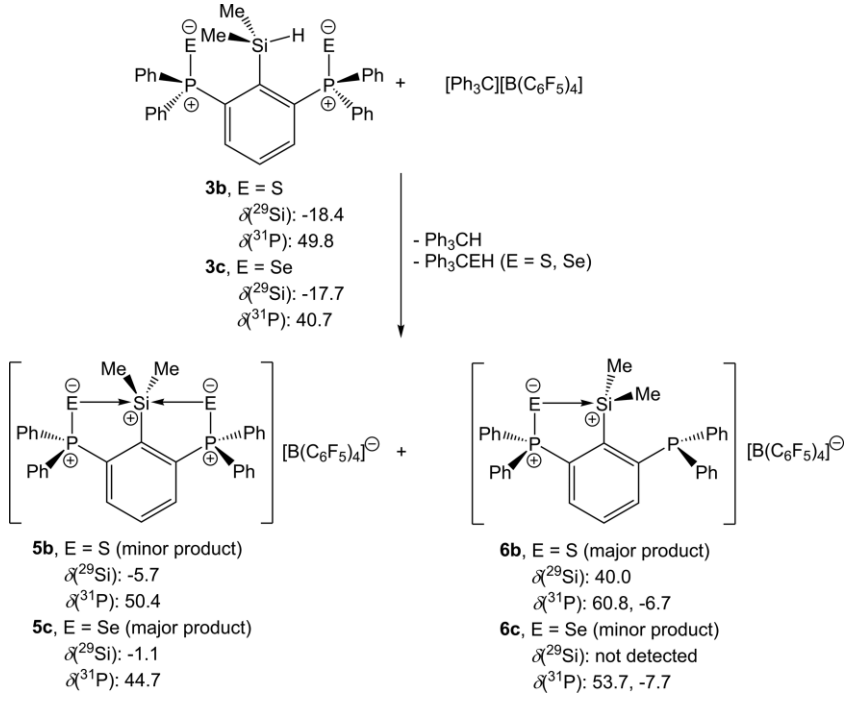

Scheme 5. Formation and selected NMR data of the E,C,E- and E,C-supported silyl cations **5b**, **5c**, **6b** and **6c** (E = S, Se).

Since all 2,6-bis(diphenylphosphinchalcogenido)dimethylsilylbenzenes 2,6-$(Ph_2PE)_2C_6H_3SiMe_2H$ (**3a**, E = O; **3b**, E = S; **3c**, E = Se) gave evidence for the partial dechalcogenation during the Bartlett–Condon–Schneider reaction, the same reaction was also extended to the unsymmetric species 2-(Ph_2PE)-6-(Ph_2P)-$C_6H_3SiMe_2H$ (**4b**, E = S; **4c**, E = Se) and $[Ph_3C][B(C_6F_5)_4]$ or $[Ph_3C][B\{(3,5\text{-}CF_3)_2C_6H_3\}_4]$, which gave the E,C-supported silyl cations $[2\text{-}(Ph_2PS)\text{-}6\text{-}(Ph_2P)C_6H_3SiMe_2]^+$ (**6b**, E = S; **6c**, E = Se) as sole products in solution with sufficient purity (Scheme 6). No indication for the dechalcogenation reaction was observed during the synthesis of **6b**. However, when **6c** was prepared by reacting **4c** with $[Ph_3C][B\{(3,5\text{-}CF_3)_2C_6H_3\}_4]$ in C_6D_6 a mixture of **6c** (major product), **5c**, and an unidentified side-product was obtained (see ESI for details). The ratio between the products of this reaction remained constant for at least 12 h. The same reaction had a different outcome when it was carried out in fluorobenzene (see ESI for details). Shortly after the start of the reaction (its progress was monitored by ^{31}P NMR) a mixture of **6c**, **5c** and an unidentified product was obtained. The starting material was consumed in less than 13 minutes, and after this time the concentration of **5c** and the unknown product decreased rapidly. Within 60 minutes the molar ratio between **6c** and **5c** became 1:0.02. While this solvent dependence is still not fully understood, the observation shows that the reaction mechanism might be quite complex. The E,C-supported silyl cations $[2\text{-}(Ph_2PE)\text{-}6\text{-}(Ph_2P)C_6H_3SiMe_2]^+$ (**6b**, E = S; **6c**, E = Se)

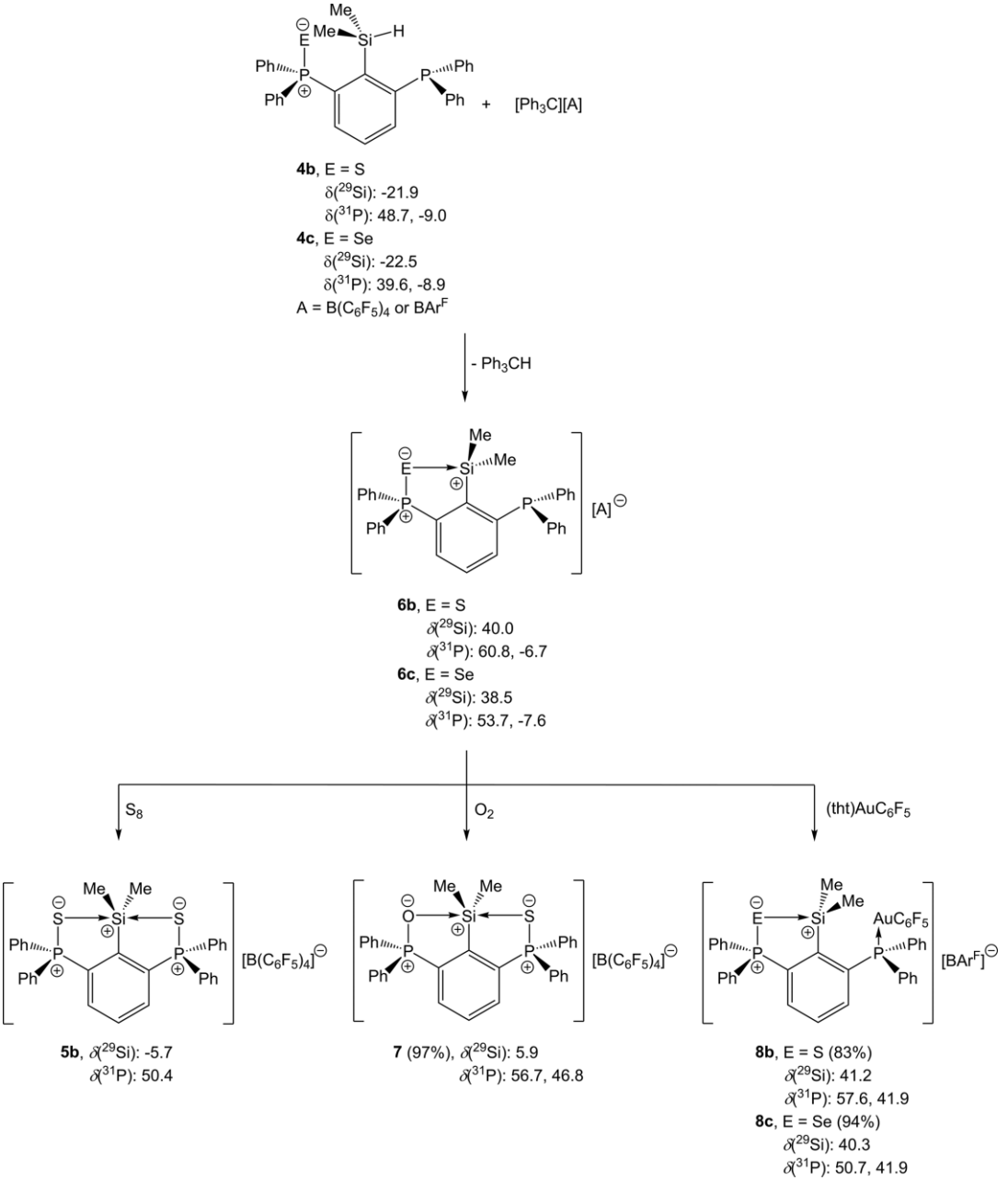

Scheme 6. Formation and selected NMR data of the E,C-supported silyl cations **6b** (E = S) and **6c** (E = Se), the S,C,E-supported silyl cations **5b** (E = S) and **7** (E = O) as well as the E,C,Au-supported silyl cations **8b** (E = S) and **8c** (E = Se).

Full Paper
doi.org/10.1002/ejic.202000800

are fairly reactive and all attempts to isolate these species were impeded by decomposition. However, the clean formation of silyl cations **6b** and **6c** was unambiguously confirmed by ^{31}P, ^{29}Si and ^{77}Se NMR spectroscopy (see below). Freshly prepared samples of **6b** and **6c** were used for all subsequent reactions. Exposed to the air, **6b** reacted rapidly with molecular oxygen to give the O,C,S-supported silyl cation $[2\text{-}(Ph_2PS)\text{-}6\text{-}(Ph_2PO)\text{-}C_6H_3SiMe_2]^+$ (**7**). The reaction of **6b** with sulfur proceeded at a slower pace (6 d), but eventually produced the S,C,S-supported silyl cation $[2,6\text{-}(Ph_2PS)_2C_6H_3SiMe_2]^+$ (**5b**).

The E,C,E′-supported silyl cations **5a**, **5b**, **5c** and **7** (E, E′ = O, S, Se) were isolated by crystallization and obtained as crystalline materials that can be handled in air for short periods of time. When solutions of **6b** and **6c** were treated with $(tht)AuC_6F_5$, the corresponding E,C,Au-supported silyl cations $[2\text{-}(Ph_2PAuC_6F_5)\text{-}6\text{-}(Ph_2PE)C_6H_3SiMe_2]^+$ (**8b**, E = S, **8c**, E = Se; counterion $[B\{3,5\text{-}(CF_3)_2C_6H_3\}_4]^-$) were obtained as crystalline air-sensitive materials in good yields (Scheme 6).

Solid-State and Solution Structure

The molecular structures of the precursors **2**, **3a**·H_2O, **3b**, **3c** and **4b**, the E,C,E′-pincer supported silyl cations **5a**, **5c** and **7** (E, E′ = O, S, Se) as well as the E,C,Au-pincer supported silyl

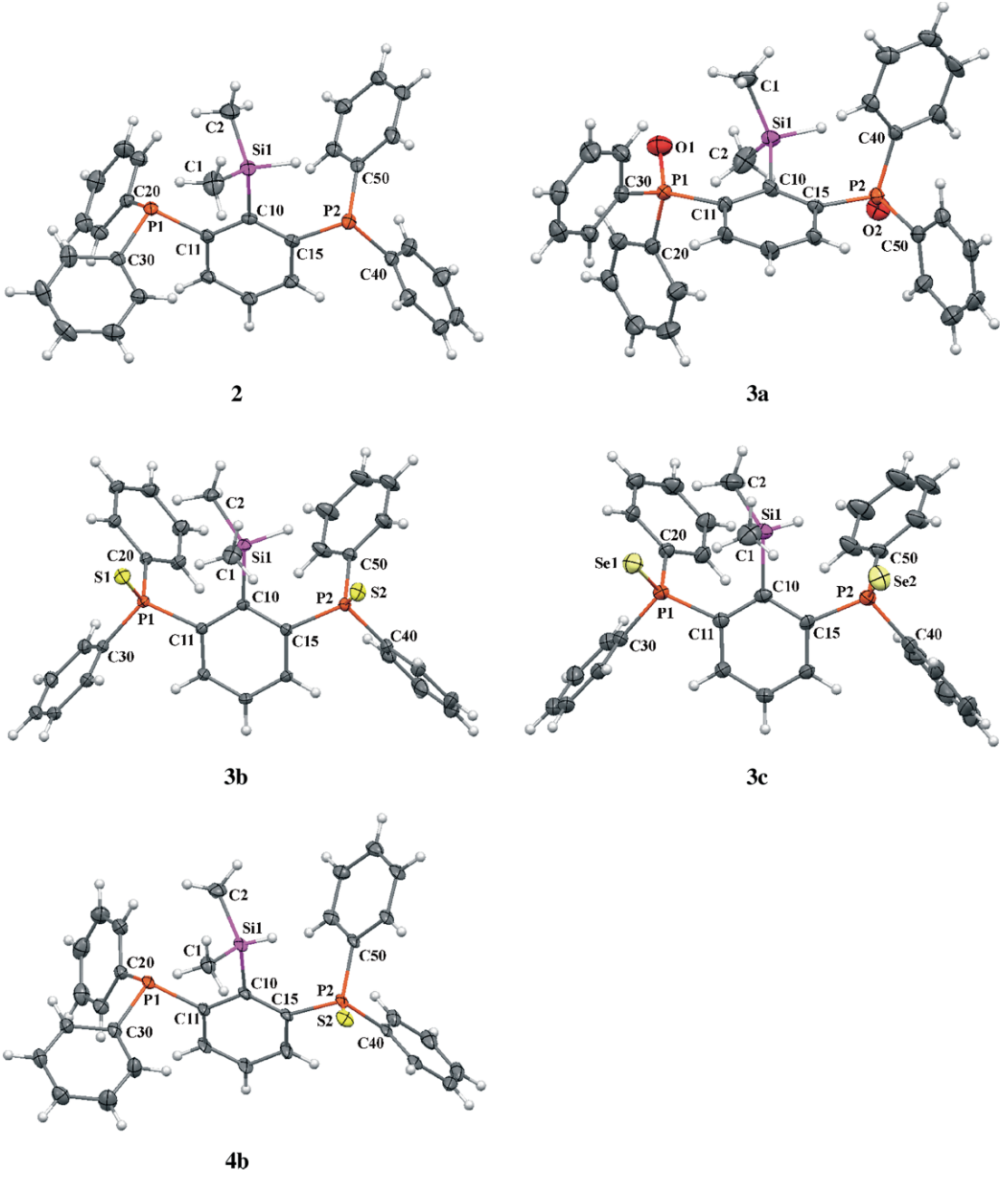

Figure 2. ORTEP view of the of X-ray molecular structure of **2**, **3a**, **3b**, **3c** and **4b** showing the atom-numbering scheme. Displacement ellipsoids are drawn at the 30 % probability level and H atoms are shown as small spheres of arbitrary radii.

Full Paper
doi.org/10.1002/ejic.202000800

cations **8b** and **8c** (E = S, Se) are shown in Figure 2, 3 and 4. Selected bond parameters are collected in Table 1. The spatial arrangement of the Si atoms of the precursors **2**, **3a**·H_2O, **3b**, **3c** and **4** is distorted tetrahedral. Only **3a** shows an intramolecular Si···O contact (3.024(8) Å) significantly longer than that of **VIII** (2.738(2) Å), which is indicative to weak σ-hole bonding.[28] The tetrahedral geometry of the Si atoms is unaffected by this additional coordination as the sum of C–Si–C angles steadily increases in the series **2** (338.1(3)°), **3a** (339.9(4)°), **3b** (341.5(1)°) and **3c** (343.6(4)°). The spatial arrangement of the Si atoms of the silyl cations **5a**, **5c** and **7** is distorted trigonal bipyramidal (type **IV**, Chart 1), whereby the three C atoms and chalcogen atoms E, E′ = O, S, Se adopt the equatorial and axial positions, respectively. The distortion is reflected in the O-Si–O angle of **5a** (168.9(2)°), which deviates remarkably from linearity. The Si–O bond lengths of **5a** (1.902(4) and 1.963(4) Å) compare well with those of **V** (1.923(1) and 1.931(1) Å). The Si–O bond length of **7** (1.825(2) Å) is significantly smaller, albeit still larger than Si–O single bonds. The Si–Se bond lengths of **5c** (2.597(3) and 2.823(3) Å) are uneven. The Si–S bond length of **7** (2.635(1) Å) lies about midway between those values. The Se–Si–Se angles of **5b** (178.2(1)°) and the O-Si–S angle of **7** (174.4(1)°) are essentially linear. The sum of C–Si–C angles of the trigonal bipyramidal silyl cations **5a** (360.0(3)°), **5c** (359.6(5)°) and **7** (358.9(1)°) is significantly higher than those of the tetrahedral precursors **2** (see above).

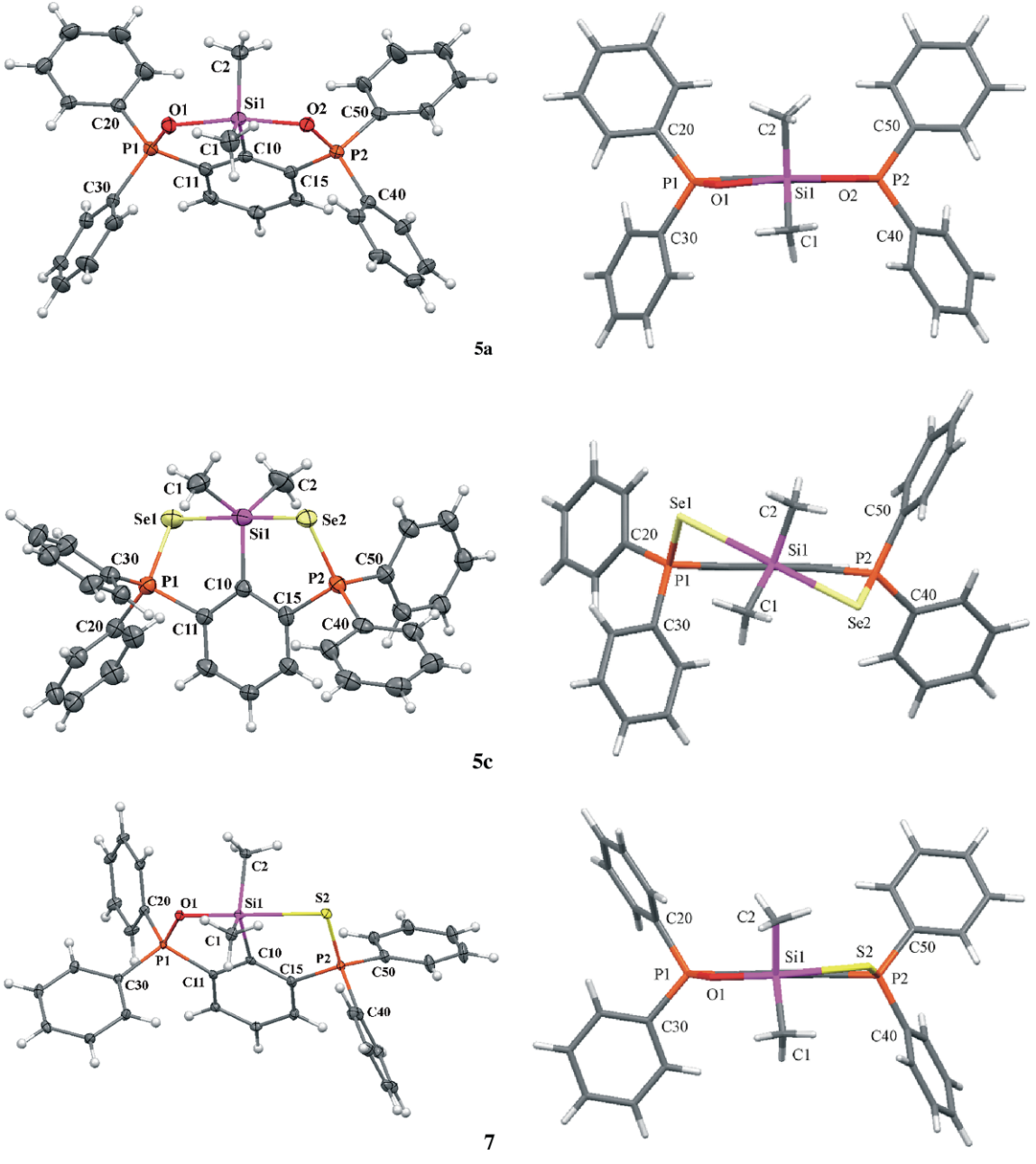

Figure 3. ORTEP view of the of X-ray molecular structure of **5a**, **5c** and **7** showing the atom-numbering scheme. Displacement ellipsoids are drawn at the 30 % probability level and H atoms are shown as small spheres of arbitrary radii.

Full Paper
doi.org/10.1002/ejic.202000800

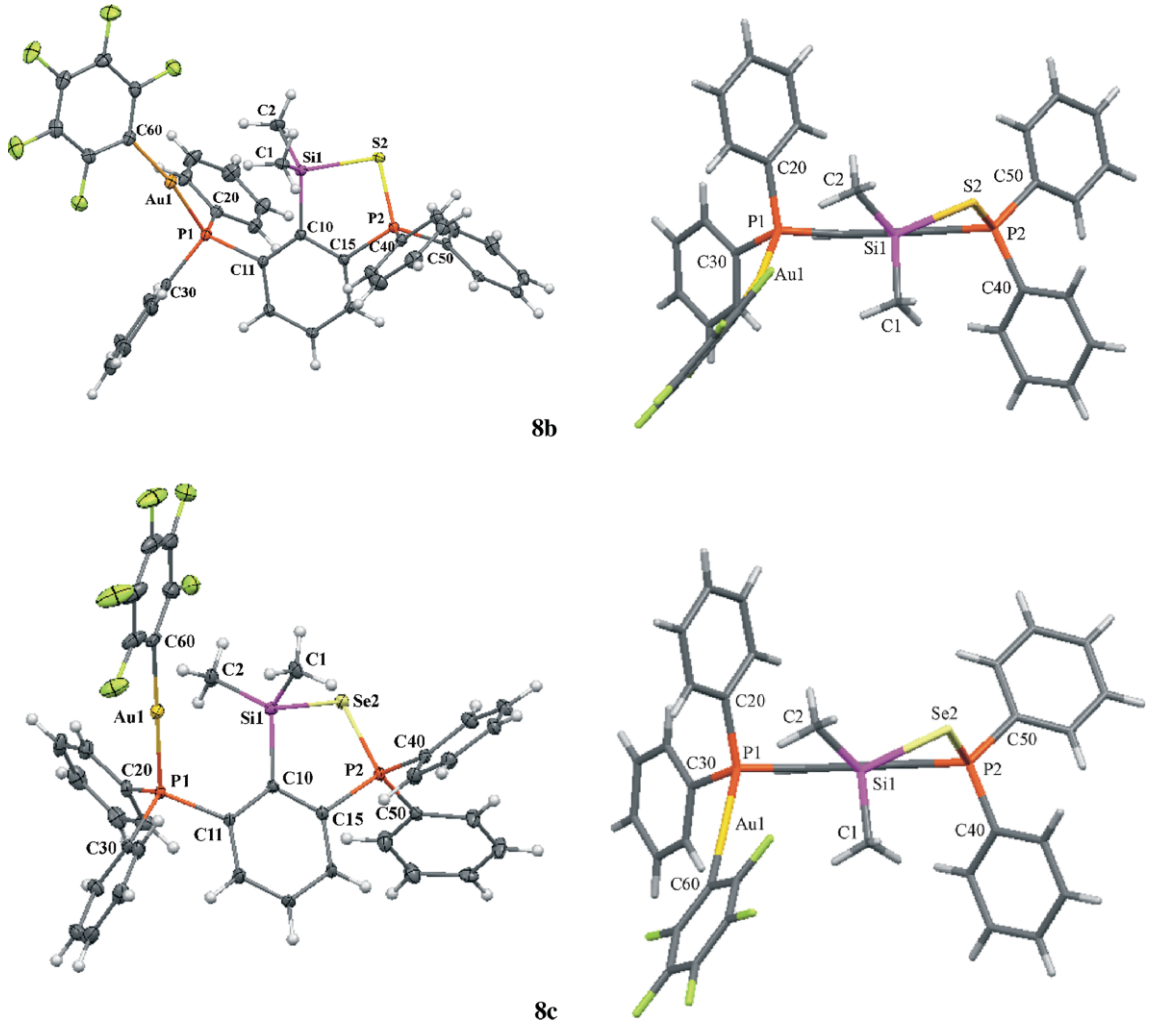

Figure 4. ORTEP view of the of X-ray molecular structure of **8b** and **8c** showing the atom-numbering scheme. Displacement ellipsoids are drawn at the 30 % probability level and H atoms are shown as small spheres of arbitrary radii.

Due to the intramolecular coordination, the P–O bond lengths of **5a** (1.525(4) and 1.525(4) Å) and **7** (1.532(2) Å) are longer than those of **3a** (1.445(6) and 1.450(6) Å). The elongation of the P–S and P–Se bonds upon intramolecular coordination is less pronounced. The spatial arrangement of the Si atoms of the silyl cations **8b** and **8c** is distorted tetrahedral (type **III**, Chart 1). The Si–S bond length of **8b** (2.216(1) Å) is significantly shorter than that of **7** (2.635(1) Å) and only slightly longer than typical Si–S single bonds. Similarly, the Si–Se bond length of **8c** (2.350(3) Å) is significantly shorter than those of **5c** (2.597(3), 2.823(3) Å) and nearly matches typical Si–Se single bonds. The Si···Au distances of **8b** (3.678(2) Å) and **8c** (3.612(5) Å) are significantly longer than the sum of van der Waals radii (approx. 3.46 and 3.56 Å),[29] which apparently suggests that there is no Si···Au interaction.

For the precursor **IX** (Scheme 2) the presence of hydrogen bridges of the Si–H···O–P type have been claimed.[17] A similar Si–H···O contact seems to be present in **3a**, as evidenced by the H···O bond length (2.826(7) Å). The other precursors **3b**, **3c** and **4b** show no evidence for contacts of the type Si–H···E interactions (E = S, Se). In the solid-state, the precursors **3a**, **3b** and **3c** each adopt different conformations regarding the position of the chalcogen atoms relative to the central C_6H_3Si plane. In **3a**·H_2O, the O atoms are situated on the opposite side of the plane (transoid), whereas in **3b** and **3c** and the S and Se atoms lie on the same sides of the plane (cisoid). In **3a**·H_2O the transoid conformation might be related to the presence of PO···H-OH hydrogen bridges. The O···O donor acceptor distances (2.844(7) and 2.907(8) Å) are indicative of medium to weak hydrogen bonding.[30] While there appears to be no Si···Au contact in **8b** and **8c**, both compounds show two intramolecular hydrogen bonds of the type C–H···Au. The H···Au bond lengths of **8b** (2.772(1) Å, 2.962(1) Å) and **8c** (2.816(2) Å, 2.891(2) Å) and the C···Au distances of **8b** (3.539(3) Å, 3.701(3) Å) and **8c** (3.555(1) Å, 3.614(1) Å) fully consistent with parameters collected for a recent survey on H···Au contacts.[31]

In the O,C,O-pincer supported silyl cation (**5a**), the O atoms are nearly coplanar with the central C_6H_3Si plane (largest deviation from the ideal plane 0.083(3) Å for O1). The same holds also for the O,C,S-pincer supported silyl cation **7** (largest deviation from the ideal plane 0.080(1) Å for S2). However, in the Se,C,Se-pincer supported silyl cation **5c**, the dimethylsilyl

Full Paper
doi.org/10.1002/ejic.202000800

Table 1. Comparison of selected bond lengths (in Å) and angles (in deg) determined by X-ray single-crystal analyses of **2**, **3a**–**3c**, **4b**, **5a**, **5c**, **7**, **8b** and **8c**.

	2	**3a**	**3b**	**3c**	**4b**	**5a**	**5c**	**7**	**8b**	**8c**
Bond lengths										
E1–Si1	–	–	–	–	–	1.963(4)	2.823(3)	1.825(2)	–	–
E2–Si1	–	–	–	–	–	1.902(4)	2.597(3)	2.635(1)	2.216(1)	2.350(3)
C1–Si1	1.891(7)	1.864(9)	1.869(2)	1.857(7)	1.864(4)	1.860(6)	1.847(9)	1.861(2)	1.847(3)	1.835(11)
C2–Si1	1.850(7)	1.867(9)	1.864(2)	1.835(8)	1.875(4)	1.850(6)	1.864(9)	1.860(2)	1.840(3)	1.846(10)
C10–Si1	1.908(5)	1.921(7)	1.931(2)	1.936(5)	1.922(4)	1.906(5)	1.926(7)	1.926(2)	1.899(3)	1.906(9)
E1–P1	–	1.450(6)	1.956(1)	2.105(2)	–	1.525(4)	2.130(2)	1.532(2)	–	–
E2–P2	–	1.445(6)	1.955(1)	2.107(2)	1.958(2)	1.525(4)	2.144(2)	1.966(1)	2.031(1)	2.178(2)
C11–P1	1.840(5)	1.816(7)	1.837(2)	1.835(6)	1.849(4)	1.790(6)	1.838(7)	1.793(2)	1.828(3)	1.835(9)
C15–P2	1.848(5)	1.829(7)	1.844(2)	1.836(5)	1.825(4)	1.792(5)	1.809(7)	1.810(2)	1.799(3)	1.800(9)
C20–P1	1.841(6)	1.819(8)	1.818(2)	1.808(6)	1.837(4)	1.793(6)	1.801(8)	1.776(2)	1.816(3)	1.806(10)
C30–P1	1.832(6)	1.811(8)	1.818(2)	1.824(6)	1.825(4)	1.795(5)	1.791(8)	1.771(2)	1.819(3)	1.801(9)
C40–P2	1.853(6)	1.814(7)	1.824(2)	1.822(7)	1.831(4)	1.786(6)	1.821(8)	1.821(2)	1.790(3)	1.788(10)
C50–P2	1.827(6)	1.807(8)	1.821(2)	1.810(7)	1.812(4)	1.781(6)	1.806(8)	1.814(2)	1.789(3)	1.797(10)
C60–Au1	–	–	–	–	–	–	–	–	2.045(3)	2.074(9)
P1–Au1	–	–	–	–	–	–	–	–	2.271(1)	2.280(2)
Bond angles										
E1–Si1–E2	–	–	–	–	–	168.9(2)	178.2(1)	174.4(1)	–	–
E1–Si1–C1	–	–	–	–	–	89.3(2)	90.7(3)	96.9(1)	–	–
E1–Si1–C2	–	–	–	–	–	95.0(2)	85.1(3)	94.1(1)	–	–
E1–Si1–C10	–	–	–	–	–	85.1(2)	87.2(2)	89.9(1)	–	–
E2–Si1–C1	–	–	–	–	–	91.1(2)	90.2(3)	88.5(1)	107.2(1)	106.0(3)
E2–Si1–C2	–	–	–	–	–	94.5(2)	95.8(3)	84.7(1)	102.8(1)	102.6(3)
E2–Si1–C10	–	–	–	–	–	85.8(2)	91.1(2)	86.2(1)	98.8(1)	98.9(3)
C1–Si1–C2	112.6(3)	117.1(4)	114.1(1)	113.6(4)	114.0(2)	118.3(3)	118.9(5)	118.7(1)	114.9(2)	115.4(5)
C1–Si1–C10	111.7(3)	109.1(4)	109.1(1)	110.1(3)	109.9(2)	127.5(3)	122.3(4)	116.3(1)	112.4(1)	112.1(4)
C2–Si1–C10	113.8(3)	113.7(4)	118.3(1)	119.9(3)	111.9(2)	114.2(3)	118.4(4)	123.9(1)	118.2(1)	118.8(4)
P1–E1–Si1	–	–	–	–	–	119.7(2)	84.2(1)	120.8(1)	–	–
P2–E2–Si1	–	–	–	–	–	121.3(2)	88.6(1)	96.9(1)	92.6(1)	87.3(1)
E1–P1–C11	–	116.0(4)	115.4(1)	115.1(2)	–	102.4(2)	104.8(2)	101.1(1)	–	–
E1–P1–C20	–	112.8(4)	114.7(1)	115.5(2)	–	111.0(2)	115.3(3)	110.5(1)	–	–
E1–P1–C30	–	110.7(4)	109.8(1)	109.7(2)	–	112.9(2)	113.7(3)	110.5(1)	–	–
E2–P2–C15	–	113.4(3)	114.7(1)	114.8(2)	113.0(1)	101.7(2)	105.6(2)	108.6(1)	105.1(1)	105.2(3)
E2–P2–C40	–	114.7(3)	111.4(1)	111.6(2)	111.4(1)	111.3(2)	112.4(2)	113.6(1)	112.4(1)	112.9(3)
E2–P2–C50	–	111.8(3)	116.0(1)	115.7(2)	116.2(1)	112.5(2)	115.0(3)	114.3(1)	110.5(1)	109.7(3)
P1–Au1–C60	–	–	–	–	–	–	–	–	170.9(1)	177.9(3)

moiety is twisted to accommodate the large Se atoms that are situated above and below the central C_6H_3Si plane (largest deviation from the ideal plane 0.353(3) Å for Se1). Similar twists are also observed for the E,C,Au supported silyl cations **8b** and **8c**.

^{29}Si NMR spectroscopy is a sensitive probe to determine the coordination number of the Si atom in solution. While truly tricoordinate silyl cations $[R_3Si^+][A^-]$ (I) show typical ^{29}Si NMR chemical shifts greater than δ = 250 ppm,[1,11] higher coordinated silyl cations **II** – **V** (Scheme 1) resonate significantly more high field. Accordingly, the O,C,O-pincer supported silyl cation **5a** gives rise to a signal at δ = –30.9 ppm, which has been high field shifted from its precursor **3a** (δ = –17.7 ppm) by about 13 pm, due to the increased coordination number. Interestingly, the S,C,S-pincer and Se,C,Se-pincer supported silyl cations **5b** and **5c** show signals at δ = –5.7 ppm and δ = –1.1 ppm, which underwent a small low field shift when compared with their precursors **3b** (δ = –18.2 ppm) and **3c** (δ = –17.7 ppm). The O,C,S-pincer supported silyl cation **7** shows a signal at δ = 5.9 ppm, while the E,C-supported silyl cations **6b** (δ = 40.0 ppm, E = S) and **6c** (δ = 38.5 ppm, E = Se) as well as the closely related E,C,Au-supported silyl cations **8b** (δ = 41.2 ppm, E = S) and **8c** (δ = 40.3 ppm, E = Se) reveal the largest ^{29}Si NMR chemical shifts of this study. The formation of **8b** and **8c** is associated with a significant shift to low fields of the resonance signal corresponding to the P(III) atom from –6.7 (for **6b**) and –7.7 ppm (for **6c**) to 41.9 ppm (for both **8b** and **8c**). The coordination of the P(III) atom to the Au(C_6F_5) moiety, gives rise to apparent quintets in ^{31}P NMR caused by coupling of ^{31}P with four ^{19}F nuclei.

Gas-Phase and Electronic Structures

Using the coordinates of the X-ray structures as starting point the gas-phase structures of the E,C,E-pincer supported silyl cations **5a**, **5b**, and **5c** (E = O, S, Se) and their precursors **2**, **3a**, **3b** and **3c** were fully optimized at the B3PW91/6-311+G(2df,p) level of theory. Due to the size and issues related to relativistic effects for the E,C,Au-pincer supported silyl cations **8b** and **8c** only single point calculations were carried out at the same level of theory. In general there is good agreement between experimental and calculated bond parameters (see ESI for details). For the precursor **3a**, both the cisoid and the transoid conformers were preliminary calculated, however, as their relative stability differs only by about 6 kJ mol^{-1} only the transoid conformer of **3a** resembling the solid-state structure most was taken into fur-

Full Paper
doi.org/10.1002/ejic.202000800

ther considerations. For **3b** and **3c** the cisoid conformers were calculated. The bond topology according to the AIM theory and isosurface representations of the ELI-D localization domains are shown in Figure 5, Figure 6, and Figure 7. Selected bond lengths and AIM bond topological parameters are collected in Table 2, whereas topological and integrated ELI-D bond descriptors are listed in Table 3. Since similar bonds exhibit similar topological and integrated RSBIs only one example is given each (see ESI for all data). The considered RSBIs include: $\rho(r)$ – the electron density at the bond critical point (bcp) – and its corresponding Laplacian ($\nabla^2\rho_{bcp}$), ε – the bond ellipticity ($\varepsilon = (\lambda_1/\lambda_2)$-1; λ_1 and λ_2 are the curvatures perpendicular to the bond axis), d_1/d – the ratio of the atom-bcp distance over the atom-atom distance, G/ρ_{bcp} and H/ρ_{bcp} – the kinetic and total energy density over ρ_{bcp} ratios,[33] V_{001} ^{ELI,} ELI_{pop} – the volume and electron population of the ELI-D basin, ELI_{max} – the ELI-D value at the attractor position, Δ_{ELI} – the distance of the attractor position perpendicular to the atom-atom axis and *RJI* – the Raub-Jansen index,[34] which provides the number of electrons (and also percentage contributions) of an bonding or lone pair ELI-D basin distributed between the adjacent AIM atoms which form a bond. The delocalization index[35] δ(A,B) is also calculated, which is a direct measure for electron sharing between two AIM atoms. In **3a**–**c** no Si–E (E = O, S, Se) bond paths were observed in the AIM topology which rules out such types of interactions in these compounds, although the Si···S distances (< 3.7 Å) and Si···Se distances (< 3.8 Å) are shorter than the sum of the Van der Waals radii of 3.9 Å and 4.0 Å, respectively. This result is supported by the AIM atomic charges (see below). However, a Si–H···O bond path was observed in **3a** indicating a weak interaction between the hydridic H atom and the also negatively

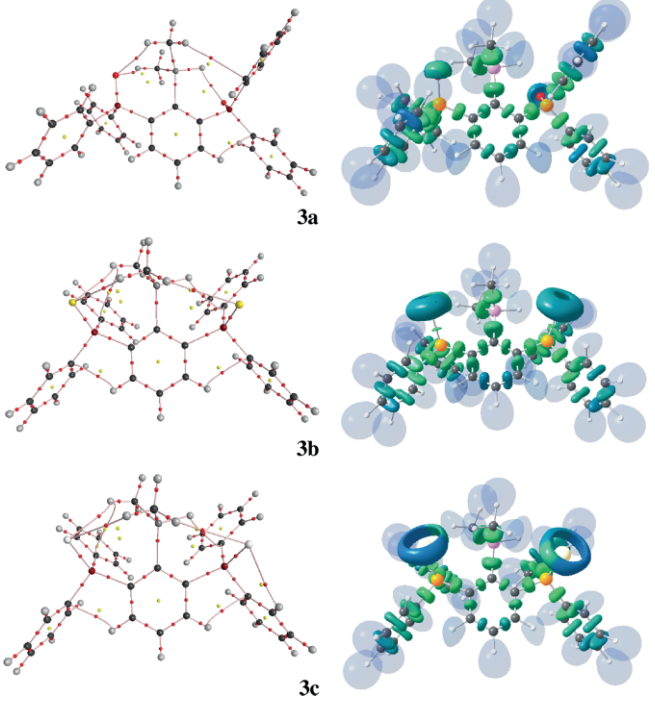

Figure 5. Left column: molecular graphs of gas-phase structures of **3a**, **3b** and **3c** (AIM2000 presentation). Right column: theoretical ELI-D localization domain representation of **3a**, **3b** and **3c**. The colour code makes domains belonging to different basins distinguishable from each other, additionally the hydrogen basins are drawn in transparent mode for clarity; *Mollso*[32] graphics at isovalue $\Upsilon = 1.50$.

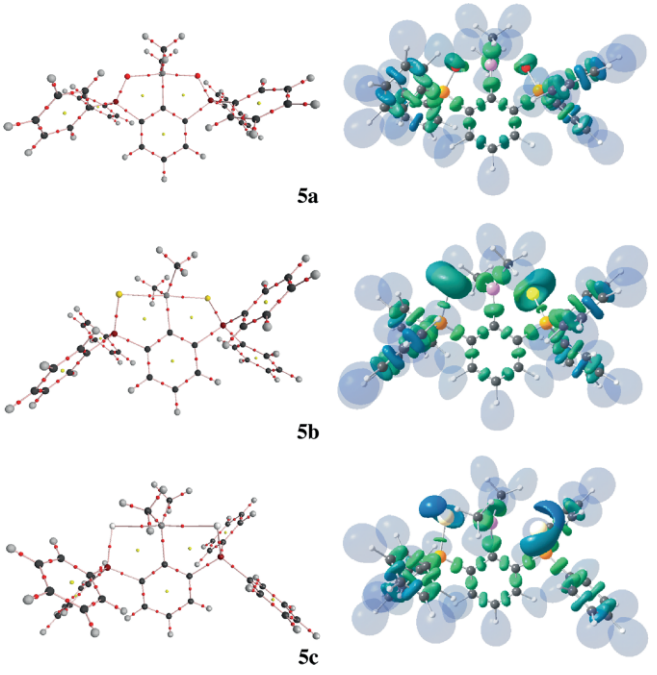

Figure 6. Left column: molecular graphs of gas-phase structures of **5a**, **5b** and **5c**. (AIM2000 presentation). Right column: theoretical ELI-D localization domain representation of **5a**, **5b** and **5c**. The color code makes domains belonging to different basins distinguishable from each other, additionally the hydrogen basins are drawn in transparent mode for clarity; *Mollso*[32]graphics at isovalue $\Upsilon = 1.50$.

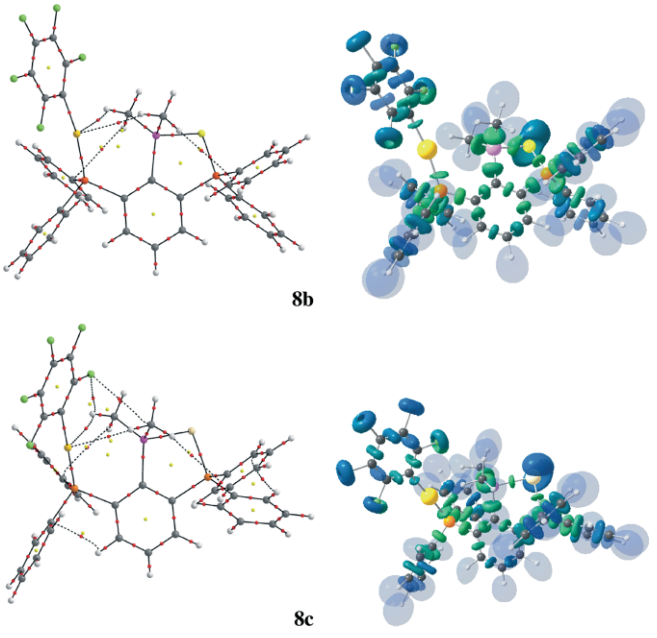

Figure 7. Left column: molecular graphs of gas-phase structures of **8b** and **8c**. (*AIMAll* presentation). Right column: theoretical ELI-D localization domain representation of **8b** and **8c**. The color code makes domains belonging to different basins distinguishable from each other, additionally the hydrogen basins are drawn in transparent mode for clarity; *Mollso*[32]graphics at isovalue $\Upsilon = 1.50$.

polarized O atom. In contrast, the molecular gas-phase structures of **5a**–**c** show such Si···E bond paths and the electronic parameters determined at the Si···E bcps unravel the respective nature of the interaction. The positive (or very close to zero) values of Laplacian at the Si–E bcps indicate polarized interactions for all three types of contacts (Table 2). As anticipated, the Si–O contacts are the shortest, leading to the highest electron density value (0.46 e/Å^3) and only in this case the Laplacian is clearly positive. The large Raub-Jansen index (*RJI* = 95 %) as well as the large G/ρ_{bcp} value (1.19 h/e) confirm the predominantly ionic character of the two Si–O bonds in **5a**, see Table 3. In contrast, the Si–S and Si–Se bonds can be considered as polarized covalent interactions as reflected in considerably negative H/ρ_{bcp} values (–0.47 h/e for **5b** and –0.41 h/e for **5c**), lower RJI values of 88 and 85 % as well as lower G/ρ_{bcp} values (0.43 h/e for **5b** and 0.31 h/e for **5c**). All other bond types listed in Table 2 and Table 3 (P–E, P/Si–C) show strong attributes of both covalent as well as ionic interactions. Generally, both types of Si–C bonds: Si–C_{sp}^3 and Si–C_{sp}^2 distances are polar covalent with quite strong polarization towards carbon atom, which is confirmed by the Raub-Jansen indexes (*RJI*) ranging between 83–89 % and the ratio H/ρ_{bcp} close to –0.7 *h/e*. The partially ionic character is confirmed by a low value of electron density at the bond critical point, a low positive value of Laplacian and a low delocalization index. All these topological and integrated parameters correspond well with literature data for C–Si linkages.[36] All C–P bonds are also polar covalent, however the polarization effect is lower in comparison to the C–Si bonds. Herein, the covalent contribution is seen from the electron density values close to 1 e/Å^3, negative values of corresponding Laplacian, and a H/ρ_{bcp} value close to –1 he^{-1}. The delocalization index unravels that more electron pairs are shared between C and P atoms (δ = 0.67–0.84, *RIJ* = 71–78 %) than for C and Si atoms (δ = 0.39–0.53, *RIJ* = 83–89 %). Aforementioned properties of C–P bond are in proper agreement with our recent results for *peri*-substituted (ace)naphthylphosphinoboranes where such type of bonds were also evaluated using both AIM and ELI-D approaches.[37]

Similarly, as it was found for the solid-state structures, the E-P bond lengths are also longer in the gas-phase E,C,E-pincer supported silyl cations (**5a**–**5c**) in comparison to those of the precursors (**2**, **3a**–**3c**), especially in case of the P–O bonds where the elongation is more pronounced due to the relatively small size of the O atom in comparison to other chalcogen atoms (S and Se). Such elongation is reflected in the topological parameters of these bonds; for example the electron density is lower in the pincer-type structures. As mentioned above, the P–O bonds are highly polarized covalent bonds with significant ionic contributions, which is consistent with findings from combined experimental and theoretical studies.[38] Herein, two parame-

Table 2. Bond length (in Å) and AIM bond topological parameters[a] for selected bonds to phosphorus and silicon atoms of **2**, **3a**–**3c**, **5a**–**5c**, **8b** and **8c**.

	Bond	*d*	ρ_{bcp}	$\nabla^2\rho_{bcp}$	d_1/d	ε	G/ρ_{bcp}	H/ρ_{bcp}
2	C1–Si1	1.8785	0.83	2.9	0.61	0.02	0.95	–0.70
8b	C1–Si1	1.847(3)	0.89	3.0	0.61	0.02	0.97	–0.73
8c	C1–Si1	1.835(11)	0.90	3.4	0.61	0.03	0.99	–0.73
2	C10–Si1	1.9155	0.78	3.1	0.62	0.03	0.95	–0.67
8b	C10–Si1	1.899(3)	0.80	3.3	0.61	0.03	0.97	–0.68
8c	C10–Si1	1.906(9)	0.79	2.8	0.61	0.03	0.96	–0.68
2	C11–P1	1.8460	1.07	–6.7	0.59	0.10	0.52	–0.96
8b	C11–P1	1.828(3)	1.11	–6.4	0.60	0.08	0.59	–1.00
8c	C11–P1	1.835(9)	1.10	–6.7	0.60	0.09	0.57	–0.99
2	C20–P1	1.8385	1.08	–6.0	0.60	0.18	0.58	–0.97
8b	C20–P1	1.816(3)	1.14	–7.3	0.60	0.09	0.56	–1.01
8c	C20–P1	1.806(10)	1.16	–7.1	0.60	0.07	0.59	–1.02
3a	P1–O1	1.4884	1.62	28.6	0.60	0.00	2.16	–0.93
5a	P1–O1	1.5323	1.47	21.7	0.60	0.06	1.93	–0.90
3b	P1–S1	1.9544	1.13	–6.2	0.54	0.01	0.36	–0.74
5b	P1–S1	1.9941	1.08	–6.2	0.55	0.08	0.31	–0.72
3c	P1–Se1	2.1103	0.93	–2.4	0.50	0.02	0.41	–0.59
5c	P1–Se1	2.1422	0.91	–2.9	0.50	0.08	0.35	–0.57
8b	P2–S2	2.031(1)	1.02	–5.9	0.55	0.08	0.29	–0.70
8c	P2–Se2	2.178(2)	0.87	–3.0	0.51	0.09	0.31	–0.55
5a	Si1–O1	1.9385	0.46	5.5	0.60	0.04	1.19	–0.34
5b	Si1–S1	2.4968	0.35	–0.2	0.63	0.05	0.43	–0.47
5c	Si1–Se1	2.6454	0.33	–0.5	0.61	0.07	0.31	–0.41
8b	Si1–S2	2.216(1)	0.57	1.1	0.64	0.04	0.74	–0.61
8c	Si1–Se2	2.350(3)	0.53	–0.6	0.65	0.04	0.55	–0.62
8b	P1–Au1	2.271(1)	0.80	2.3	0.52	0.02	0.67	–0.47
8c	P1–Au1	2.280(2)	0.79	2.2	0.51	0.01	0.66	–0.47
8b	C60–Au1	2.045(3)	0.92	3.9	0.54	0.04	0.78	–0.48
8c	C60–Au1	2.074(9)	0.88	3.6	0.54	0.03	0.75	–0.46

[a] Electron density ρ_{bcp} in e Å^{-3} and its corresponding Laplacian $\nabla^2\rho_{bcp}$ in e Å^{-5}, d_1/d – longer distance from bond critical point to nucleus over distance ratio, ε – the bond ellipticity, G/ρ_{bcp} and H/ρ_{bcp} – kinetic and total energy density over ρ_{bcp} ratios in he^{-1}.

Full Paper
doi.org/10.1002/ejic.202000800

Table 3. Topological[a] and integrated[b] ELI-D bond descriptors for selected bonds to phosphorus and silicon atoms of **2**, **3a**–**3c**, **5a**–**5c**, **8b** and **8c**.

	Bond	δ	V_{001} ^{ELI}	ELI_{pop}	ELI_{max}	Δ_{ELI}	*RJI* [e]	*RJI* [%]
2	C1–Si1	0.50	5.79	2.00	1.98	0.041	1.71	85
8b	C1–Si1	0.52	5.67	2.01	1.95	0.006	1.68	84
8c	C1–Si1	0.53	5.57	2.01	1.94	0.012	1.69	84
2	C10–Si1	0.45	8.14	2.32	2.07	0.021	2.06	89
8b	C10–Si1	0.45	7.89	2.33	2.07	0.076	2.06	88
8c	C10–Si1	0.46	7.81	2.32	2.06	0.066	2.04	88
2	C11–P1	0.84	4.99	2.14	1.89	0.038	1.64	77
8b	C11–P1	0.77	5.10	2.19	1.94	0.006	1.70	77
8c	C11–P1	0.77	5.13	2.19	1.94	0.015	1.69	77
2	C20–P1	0.84	4.86	2.14	1.89	0.065	1.67	78
8b	C20–P1	0.80	5.29	2.20	1.91	0.040	1.65	75
8c	C20–P1	0.80	5.19	2.21	1.92	0.040	1.66	75
3a	P1–O1	0.86	2.02	1.59	1.45	0.144	1.21	76
5a	P1–O1	0.72	1.74	1.53	1.49	0.038	1.25	81
3b	P1–S1	1.36	4.38	2.00	1.53	0.026	1.13	56
5b	P1–S1	1.17	4.15	1.93	1.59	0.065	0.98	51
3c	P1–Se1	1.39	5.61	2.15	1.53	0.060	1.39	65
5c	P1–Se1	1.21	5.12	2.03	1.59	0.104	1.22	60
8b	S2–P2	1.05	3.89	1.84	1.62	0.050	0.98	53
8c	Se2–P2	1.11	4.76	1.92	1.62	0.069	1.08	56
5a	Si1–O1	0.22	1.82	1.41	1.56	0.022	1.34	95
5b	Si1–S1	0.27	3.97	1.42	1.64	0.069	1.25	88
5c	Si1–Se1	0.30	4.31	1.38	1.50	0.025	1.17	85
8b	Si1–S2	0.41	4.41	1.70	1.68	0.044	1.47	86
8c	Si1–Se2	0.45	5.01	1.73	1.62	0.030	1.43	83
8b	P1–Au1	0.98	8.27	2.13	1.63	0.392	1.60	75
8c	P1–Au1	0.96	8.09	2.11	1.61	0.309	1.57	74
8b	C60–Au1	0.93	7.63	2.05	1.65	0.088	1.67	82
8c	C60–Au1	0.91	7.24	1.99	1.66	0.026	1.63	82

[a] ELI_{max} – ELI-D value at the attractor position, Δ_{ELI} – the distance in Å of the attractor position perpendicular to the atom-atom axis. [b] δ – the delocalization index, V_{001} ELI^- is the volume of the ELI-D basin in $Å^3$ cut at 0.001au, ELIpop – the electron population within the ELI-D basin in *e*, and *RJI* – the Raub-Jansen index in *e* and %.

ters: H/ρ_{bcp} and the Raub-Jansen index, showing the degree of covalency, are very similar for the P–O bond type. The values 1.93 and 2.16 he^{-1} of the parameter G/ρ_{bcp}, the highest observed for all structures analyzed, indicate the high degree of iconicity for such type of bond. Based on DFT studies combined with AIM and ELI-D approaches, P–S and P–Se bonds can be classified as shared-shell interactions with a negative value of the Laplacian and a negative H/ρ_{bcp} ratio. The P–Se bonding shows only a slight polarization towards the phosphorus atom which is reflected by *RJI* = 60–65 %. In both cases a delocalization index higher than 1 indicates that the P and S/Se atoms share more than one but less than two electron pairs. The ionic contribution described by G/ρ_{bcp} is very small and comparable to those found for P–C bonds. In the E,C,Au-pincer supported silyl cations **8b** and **8c** the nature of the C–Si/C–P/E–P bonds remains unchanged in comparison to the E,C,E supported silyl cations **5a**–**5c**, which is confirmed by the very similar real-space bonding indicators characteristic for polar-covalent interactions. Interestingly, the Si–E (E = S, Se) bond lengths are significantly shorter in **8b** and **8c** (up to 0.3 Å) in comparison to the related gas-phase structures of the E,C,E-pincer supported silyl cations **5b** and **5c**. This discrepancy is not an effect of different computational techniques used (single point calculation vs. geometry optimization) since the X-ray analysis revealed the same tendency for experimental distances of **5c** and **8c**. Such a difference in bond lengths, however, has a considerable impact on topological (ρ_{bcp}, G/ρ_{bcp}, H/ρ_{bcp}) and integrated (δ) parameters, however the Laplacian values still remain close to zero. Considering the ELI-D bonding indicators of Si–Se contact in **8c**, it is interesting to note that the electrons within its ELI-D basin are more localized (values of ELI_{max} and ELI_{pop} increased) than in structure **5c**. It is reflected in the graphical representation of ELI-D isosurfaces of **8c** and **5c**. In the former case (Figure 7) the Si1–Se2 basin is clearly visible in contrast to the latter case (Figure 6) where the corresponding basin is not observed at Y = 1.5 (but becomes visible at smaller ELI-D values). For the related Si–S basins of **5b** and **8b** the enhancement of electron localization is not so clearly pronounced. Interestingly in all studied S, Se-pincer supported cations, the RJIs remain comparable (above 80 %) confirming the polar covalent character of studied Si–E (E = S, Se) contacts. The AIM analysis confirmed the existence of intramolecular C–H···Au interactions found in the crystal structures of **8b** and **8c**. The topological properties determined at the Au···H bond critical points clearly show that these interactions are weak with electron density close to zero (0.06–0.09 $e\ Å^{-3}$), the associated Laplacian below $1e\ Å^{-5}$, and the kinetic energy density dominates the potential energy density ($|V|/G$ = 0.85–0.88).[33]

Full Paper
doi.org/10.1002/ejic.202000800

Table 4. Selected atomic charges (in *e*) of **2**, **3a**-**3c**, **5a**, **5c**, **8b** and **8c**.

		E1	E2	Si	P1	P2	(Si)H	Σ(Ph_2P1)	Σ(Ph_2P2)	ΣPh(10–15)
2		–	–	2.77	1.47	1.46	–0.67	0.48	0.47	–1.65
3a	E = O	–1.49	–1.48	2.77	2.93	2.91	–0.67	1.97	1.97	–1.66
3b	E = S	–0.74	–0.73	2.76	2.02	1.99	–0.67	1.15	1.12	–1.52
3c	E = Se	–0.47	–0.47	2.76	1.72	1.69	–0.67	0.87	0.85	–1.48
5a	E = O	–1.54	–1.54	2.91	2.92	2.92	–	2.08	2.08	–1.66
5b	E = S	–0.78	–0.78	2.65	2.16	2.16	–	1.40	1.40	–1.58
5c	E = Se	–0.48	–0.48	2.56	1.89	1.89	–	1.14	1.14	–1.56
8b	E2 = S	–	–0.88	2.77	1.75	2.23	–	0.93	1.50	–1.61
8c	E2 = Se	–	–0.59	2.70	1.79	1.99	–	0.94	1.26	–1.60

Analysis of AIM Charges

Selected atomic and fragmental charges obtained by integration of the AIM atomic basins are given in Table 4. As anticipated, the chalcogen atoms are negatively charged according to the relative electronegativities: O (–1.48 *e* to –1.54 *e*) > S (–0.73 *e* to –0.78 *e*) > Se (–0.47 *e* to –0.48 *e*) while the Si and P atoms are significantly positive (2.56 *e* to 2.91 *e* for Si, 1.47 e to 2.92 e for P). In the three precursors **3a**–**c** the Si charges remain constant at about 2.76 *e* and the H(Si) charges remain constant at –0.67 e. The P atoms solely compensate the negative charges of the E atoms. Hence, in accordance with the geometrical and other real-space bonding indicators, Si–E or Si–H···E/P interactions are not observed for the precursors **3a**–**c**.

However, due to the obvious Si–E interactions in the E,C,E-pincer supported silyl cations **5a**–**c** distinct changes in the AIM atomic charges are observed in comparison to the corresponding precursors. Interestingly, in **5a** the Si atom has 0.14 *e* less electrons compared to its precursor **3a**, whereas an electron increase of 0.11 *e* and 0.20 *e* is found for the corresponding S- and Se-containing pincer molecules **5b** and **5c**.

Conclusions

A versatile route for the preparation of E,C,E′-pincer type supported silyl cations, such as $[2,6\text{-}(Ph_2PE)_2C_6H_3SiMe_2]^+$ (**5a**, E = O; **5b**, E = S; **5c**, E = Se), $[2\text{-}(Ph_2PS)\text{-}6\text{-}(Ph_2PO)C_6H_3SiMe_2]^+$ (**7**) and $[2\text{-}(Ph_2PAuC_6F_5)\text{-}6\text{-}(Ph_2PE)C_6H_3SiMe_2]^+$ (**8b**, E = S; **8c**, E = Se) has been developed. The relative coordination number according to the ^{29}Si NMR chemical shifts decreases in the order **5a** (–30.9 ppm) < **5b** (–5.7 ppm) < **5c** (–1.1 ppm) < **7** (5.9 ppm) < **8c** (40.3 ppm) ≈ **8b** (41.2 ppm). The nature of the intramolecularly coordinating chalcogen atoms E was analyzed by an electron density based set of RSBIs derived from the AIM and ELI-D space partitioning schemes Consistent with the aforementioned trend regarding the relative coordination number, the kinetic energy density over ρ_{bcp} ratios reveal that the strength of the Si–E bonds decreases in the order **5a** (1.19 he^{-1}) < **5b** (0.43 he^{-1}) < **5c** (0.31 he^{-1}). Several other RSBIs including the electron density and its Laplacian at the bond critical point (bcp) as well as the Raub Jansen index (RJI) suggest that the Si–O bond is ionic in nature, which is in line with the large electronegativity difference of both elements.[20] In contrast, the Si–S and Si–Se bonds are slightly less ionic, which is also consistent with smaller electronegativity difference of these elements. While all tricoordinate silyl cations **I** are highly reactive Lewis acids, the O,C,O-supported silyl cation **5a** is air-stable not even showing any reactivity towards the oxidizing and rather nucleophilic counterion Br_3^-. In the E,C,E′-pincer type supported silyl cations, high positive charges are also situated on the P atoms of **5a** (2.92 e), **5b** (2.16 e) and **5c** (1.89 e), which can be accounted for the by use of bipolar single bonds $^+$P–E$^-$ in the Lewis formula representations (Scheme 2, Scheme 3, Scheme 4, Scheme 5, and Scheme 6). In this way, both Si and P atoms are assigned formal positive charges. In light of the recent controversial debate of the appropriate description of donor acceptor bonds within main group compounds,[19] we deliberately used "arrows" to emphasize the strongly polar or even ionic bond character of the Si–O bond in **5a**. Resonance structures involving "formal charges" suggesting a higher degree of covalence, are rather inadequate to describe the bond situation of the Si–O bonds of **5a**. The same holds true for the Si–S bonds of **5b** and the Si–Se bonds of **5c**, albeit the bond polarity of these bonds is less pronounced. In an effort to contribute to this debate[19] we propose to generally write donor–acceptor complexes with predominately covalent bond character using "lines and formal charges" and those with predominately ionic bond character using "arrows".

Experimental Section

General. Reagents were obtained commercially and used as received. Dry solvents were collected from a SPS800 mBraun solvent system. Triphenylcarbenium tetrakis(pentafluorophenyl)borate,[8] triphenylcarbenium tetrakis[3,5-bis(trifluoromethyl)phenyl]borate,[39] (tht)AuC_6F_5,[40] and dimethylsilyl-2,3-dibromobenzene[26] were prepared according to literature procedures. ^{1}H-, ^{13}C-,^{29}Si-, ^{77}Se and ^{31}P-NMR spectra were recorded in $CDCl_3$ unless otherwise stated at r.t. using Bruker Avance 360 and Bruker Avance DPX 200 spectrometers and are referenced to tetramethylsilane (^{1}H, ^{13}C, ^{29}Si), phosphoric acid 85 % in water (^{31}P), $CFCl_3$ (^{19}F), Ph_2Se_2 (^{77}Se). Chemical shifts are reported in parts per million (ppm) and coupling constants (*J*) are given in Hertz (Hz). Electron impact mass spectroscopy (EIMS) was carried out using a Finnigan MAT 95. The ESI MS spectra were obtained with a Bruker Esquire-LC MS. Methanol solutions (unless otherwise stated, $c = 1 \times 10^{-6}$ mol L^{-1}) were injected directly into the spectrometer at a flow rate of 3 μL min^{-1}. Nitrogen was used both as a drying gas and for nebulization with flow rates of approximately 5 L min^{-1} and a pressure of 5 psi, respectively. Pressure in the mass analyzer region was usually about 1×10^{-5} mbar. Spectra were collected for one minute and averaged.

Synthesis of $2,6\text{-}F_2C_6H_3SiMe_2H$ (1a). A 2.5-M solution of *n*-butyllithium (21.9 mmol, 8.8 mL) in THF (40 mL) and *n*-hexane (18 mL)

was cooled down to –78 °C and diisopropylamine (2.2 g, 21.9 mmol) and 1,3-difluorobenzene (2.5 g, 21.9 mmol) was successively added. The mixture was stirred 1 h at –78 C then dimethylchlorosilane (2.1 g, 21.9 mmol) in THF (10 mL) was added dropwise. After 1 h stirring at –78 °C the reaction was quenched with distilled water. The layers were separated, the aqueous layer was extracted with CH_2Cl_2 and the combined organic layers were dried with $MgSO_4$. The solvents were removed at reduced pressure to leave a yellow oil. Vacuum trap to trap condensation afforded **1a** as colorless oil (2.6 g, 15.1 mmol, 69 %).

^{1}H-NMR (200 MHz, $CDCl_3$): δ = 7.40–7.27 (m, 1H), 6.89–6.78 (m, 2H), 4.64 (sept, 1H, $^3J(^1H\text{-}^1H)$ = 4 Hz, $^1J(^{29}Si\text{-}^1H)$ = 155 Hz), 0.45 (m, 6H). $^{13}C\{^1H\}$-NMR (50 MHz, $CDCl_3$): δ = 167.2 (dd, $^1J(^{19}F\text{-}^{13}C)$ = 244Hz, $^3J(^{19}F\text{-}^{13}C)$ = 15Hz), 132.4 (t, $^3J(^{19}F\text{-}^{13}C)$ = 10Hz), 111.0 (dd, $^2J(^{19}F\text{-}^{13}C)$ = 27 Hz, $^4J(^{19}F\text{-}^{13}C)$ = 2 Hz), –3.4 ppm. ^{19}F-NMR (188 MHz, $CDCl_3$): δ = –99.2. $^{29}Si\{^1H\}$-NMR (72 MHz, $CDCl_3$): δ = –26.2 (t, $^3J(^{19}F\text{-}^{29}Si)$ = 8 Hz). IR (KBr): $\tilde{\nu}$(Si-H) = 2161 cm^{-1}. MS (EI): *m/z* = 172 [M]$^+$.

Synthesis of 2,6-(Ph_2P)$_2C_6H_3SiMe_2H$ (2). Method A. A suspension of lithium granule (0.21 g, 30 mmol) in THF (20 mL) and diphenylchlorophosphine (3.6 g, 16.6 mmol) were stirred at room temperature until the lithium granules were consumed. The solution turned dark red shortly after the beginning of the reaction. Neat **1a** (1.0 g, 5.8 mmol) was added and the mixture was stirred overnight at room temperature. The solvent was removed under reduced pressure and the residue was washed with acetonitrile (50 mL). To separate the lithium chloride from the product, dichloromethane (50 mL) was added and the suspension filtered. The solvent was removed in vacuo to give colorless crystals of **2** (2.6 g, 5.3 mmol, 91 %; Mp. 155 °C).

Method B. A 2.5-M solution of *n*-butyllithium (27.2 mL, 68.0 mmol) in diethyl ether (250 mL) was cooled to –78 °C. N,N,N′,N′-tetramethylethylenediamine (7.90 g, 68.0 mmol) and **1b** (10.0 g, 34.0 mmol) were added and stirring was continued for 2 h at –78 °C.

The solution was warmed up to room temperature and chlorodiphenylphosphine (15.0 g, 68.0 mmol) in diethyl ether (25 mL) was added drop wise. The mixture was stirred overnight. The solvent was removed under reduced pressure and the residue was washed with acetonitrile (50 mL). To separate the lithium chloride from the product, dichloromethane (50 mL) was added and the suspension filtered. The solvent was removed in vacuo to give colorless crystals of **2** (12.5 g, 24.8 mmol, 73 %; Mp 155 °C).

^{1}H-NMR (200 MHz, $CDCl_3$): δ = 7.36–6.98 (m, 23H), 5.29 (sept, 1H, $^3J(^1H\text{-}^1H)$ = 4 Hz), $^1J(^{29}Si\text{-}^1H)$ = 185 Hz), 0.32 (dt, 6H, $^3J(^1H\text{-}^1H)$ = 4Hz, $^3J(^{31}P\text{-}^{13}H)$ = 4Hz). $^{13}C\{^1H\}$-NMR (50 MHz, $CDCl_3$): δ = 151.8 (t,$^2J(^{31}P\text{-}^{13}C)$ = 39 Hz) 145.5 (dd, *J* = 15, 13 Hz), 138.2 (d, *J* = 12 Hz), 134.6 (s), 133.9 (d, *J* = 20 Hz), 129.4, 128.8–128.4 (multiple signals overlapped), –0.5 (t, $^4J(^{31}P\text{-}^{13}C)$ = 11 Hz). $^{29}Si\{^1H\}$-NMR (72 MHz, $CDCl_3$): δ = –24.8 (t, $^3J(^{31}P\text{-}^{29}Si)$ = 23 Hz). $^{31}P\{^1H\}$-NMR (81MHz, $CDCl_3$): δ = –6.2 (s, $^3J(^{29}Si\text{-}^{31}P)$ = 23 Hz). IR (KBr): $\tilde{\nu}$(Si-H) = 2171 cm^{-1}. MS (EI): *m/z*: = 504 [M]$^+$. MS (ESI$^+$)**:** *m/z*: = 505 [M + H]$^+$, 527 [M + Na]$^+$, 543 [M + K]$^+$.

Synthesis of 2,6-(Ph_2PO)$_2C_6H_3SiMe_2H$ (3a). A solution of **2** (0.60 g, 1.20 mmol) and hydrogen peroxide urea adduct (0.23 g, 2.40 mmol) in THF (10 mL) was stirred for 1 h at room temperature. The solvent was removed and the white precipitate was washed with dichloromethane. The solvent was removed under reduced pressure and the crude product was recrystallized from dichloromethane as colorless crystals of **3a** (550 mg, 1.1 mmol, 93 %; Mp. 109 °C).

^{1}H-NMR (200 MHz, $CDCl_3$): δ = 7.64–7.16 (m, 23H), 4.93 (sept, 1H, $^3J(^1H\text{-}^1H)$ = 4 Hz, $^1J(^{29}Si\text{-}^1H)$ = 181 Hz), 0.22 (d, 6H, $^3J(^1H\text{-}^1H)$ = 4 Hz, $^2J(^{29}Si\text{-}^1H)$ = 123 Hz). $^{13}C\{^1H\}$-NMR (50 MHz, $CDCl_3$): δ = 152.3, 141.0 (dd, *J* = 104, 13 Hz), 136.7 (m), 134.4 (d, $^1J(^{31}P\text{-}^{13}C)$ = 103.5 Hz), 132.1 (d, *J* = 10.0 Hz), 131.8, 128.6 (d, *J* = 26 Hz), –0.9. $^{29}Si\{^1H\}$-NMR (72 MHz, $CDCl_3$): δ = –17.65 (t, $^3J(^{31}P\text{-}^{29}Si)$ = 6 Hz). $^{31}P\{^1H\}$-NMR (81 MHz, $CDCl_3$): δ = 34.8 (s,$^1J(^{13}C\text{-}^{31}P)$ = 104 Hz). IR (KBr): $\tilde{\nu}$(Si-H) = 2190 cm^{-1}. MS (EI): *m/z* = 535 [M – H]$^+$.

Synthesis of 2,6-(Ph_2PE)$_2C_6H_3SiMe_2H$ (E = S, 3b; E = Se, 3c). A suspension of **2** (2.02 g, 4.0 mmol) and the appropriate chalcogen (257 mg of S_8 or 632 mg of Se_8, 8.0 mmol) in THF (5 mL) was stirred 15 h at room temperature. The solution was filtered and the solvent was removed. Recrystallization from dichloromethane/*n*-hexane (1:3) afforded colorless crystals of **3b** (2.05 g, 3.6 mmol, 89 %, mp. 195 °C) and yellow crystals of **3c** (2.05 3.1 mmol, 78 %; Mp. 203 °C).

3b: ^{1}H-NMR (200 MHz, $CDCl_3$): δ = 7.74–7.10 (m, 23H), 5.1 (sept, 1H, $^3J(^1H\text{-}^1H)$ = 4 Hz, $^1J(^{29}Si\text{-}^1H)$ = 190 Hz), 0.14 (d, 6H, $^3J(^1H\text{-}^1H)$ = 4 Hz, $^2J(^{29}Si\text{-}^1H)$ = 123 Hz). $^{13}C\{^1H\}$-NMR (50 MHz, $CDCl_3$): δ = 151.2 (t, *J* = 20 Hz), 143.5 (dd, $^1J(^{31}P\text{-}^{13}C)$ = 86 Hz, $^3J(^{31}P\text{-}^{13}C)$ = 14 Hz), 136.7 (dd, *J* = 16, 4 Hz), 135.1 (d, $^1J(^{31}P\text{-}^{13}C)$ = 85 Hz), 132.3 (d, *J* = 10 Hz), 131.5, 128.6 (d, *J* = 13 Hz), 127.2 (t, *J* = 26 Hz), 1.2. $^{29}Si\{^1H\}$-NMR (72 MHz, $CDCl_3$): δ = –18.4 (t, $^3J(^{31}P\text{-}^{29}Si)$ = 8 Hz). $^{31}P\{^1H\}$-NMR (81 MHz, $CDCl_3$): δ = 49.8 (s, $^1J(^{13}C\text{-}^{31}P)$ = 85 Hz). IR (KBr): $\tilde{\nu}$(Si-H) = 2223 cm^{-1}. MS (EI): *m/z* = 567 [M – H]$^+$.

3c: ^{1}H-NMR (200 MHz, $CDCl_3$): δ = 7.80–7.06 (m, 23H), 5.26 (sept, 1H, $^3J(^1H\text{-}^1H)$ = 4 Hz, $^1J(^{29}Si\text{-}^1H)$ = 191 Hz), 0.13 (d, 6H, $^3J(^1H\text{-}^1H)$ = 4 Hz, $^2J(^1H\text{-}^{29}Si)$ = 123 Hz). $^{13}C\{^1H\}$-NMR (50 MHz, $CDCl_3$): δ = 151.6 (t, *J* = 19 Hz), 143.5 (dd, $^1J(^{31}P\text{-}^{13}C)$ = 77 Hz, $^3J(^{31}P\text{-}^{13}C)$ = 14 Hz), 136.4 (dd, *J* = 16, 4 Hz), 133.6 (d, *J* = 79 Hz), 132.8 (d, *J* = 10 Hz), 131.5, 128.6 (d, *J* = 13 Hz), 127.4 (t, *J* = 13 Hz), 1.0 (s, $^1J(^{29}Si\text{-}^{13}C)$ = 28 Hz). $^{29}Si\{^1H\}$-NMR (72 MHz, $CDCl_3$): δ = –17.7 (t, $^3J(^{31}P\text{-}^{29}Si)$ = 21 Hz). $^{31}P\{^1H\}$-NMR (81 MHz, $CDCl_3$): δ = 40.7 (s, $^1J(^{77}Se\text{-}^{31}P)$ = 725 Hz). $^{77}Se\{^1H\}$-NMR (69 MHz, $CDCl_3$): δ = –207.5 (d, $^1J(^{31}P\text{-}^{77}Se)$ = 725 Hz). IR (KBr): $\tilde{\nu}$(Si-H) = 2220 cm^{-1}. MS (EI): *m/z* = 663 [M – H]$^+$.

Synthesis of 2-(Ph_2PS)-6-(Ph_2P)-$C_6H_3SiMe_2H$ (4b). A solution of **2** (2.0 g, 4.0 mmol) and sulfur (128 mg, 4.0 mmol) in THF (5 mL) was stirred for 15 h at room temperature. The suspension was filtered and the solvent was removed. Recrystallization from dichloromethane/*n*-hexane (1:3) afforded colorless crystals of **4b**. (2.1 g, 3.9 mmol, 98 %; Mp. 178 °C). Alternatively, **4b** can be purified by column chromatography with *n*-hexane/$CHCl_3$ (4:1.5) using aluminum oxide as stationary phase.

^{1}H-NMR (200 MHz, $CDCl_3$): δ = 7.85–7.74 (m, 4H), 7.48–6.99 (m, 20H) 5.01 (m, 1H), 0.40 (t, 6H, *J* = 4 Hz). $^{13}C\{^1H\}$-NMR (50 MHz, $CDCl_3$): δ = 152.6 (dd, $^1J(^{31}P\text{-}^{13}C)$ = 50 Hz, $^3J(^{31}P\text{-}^{13}C)$ = 17 Hz), 147.6 (apparent t, *J* = 14 Hz), 141.7 (dd, $^1J(^{31}P\text{-}^{13}C)$ = 86 Hz, $^3J(^{31}P\text{-}^{13}C)$ = 16 Hz), 138.5 (d, *J* = 2 Hz), 137.7 (d, *J* = 11 Hz), 135.3, 134.3, 134.0, 133.7, 133.2 (d, *J* = 18 Hz), 132.4 (d, *J* = 10 Hz), 131.3 (d, *J* = 3 Hz), 128.7, 128.6. 129.5, 128.3, –0.1 (d, $^4J(^{31}P\text{-}^{13}C)$ = 20 Hz). $^{29}Si\{^1H\}$-NMR (72 MHz, $CDCl_3$): δ = –21.9 (t, $^3J(^{31}P\text{-}^{29}Si)$ = 10 Hz). $^{31}P\{^1H\}$-NMR (81 MHz, $CDCl_3$): δ = 48.7 (d, $^4J(^{31}P\text{-}^{31}P)$ = 4 Hz), –9.0 (d, $^4J(^{31}P\text{-}^{31}P)$ = 4 Hz). IR (KBr): $\tilde{\nu}$(Si-H) = 2201 cm^{-1}. MS (EI): *m/z* = 535 [M – H]$^+$, 503 [M–SH]$^+$.

Synthesis of 2-(Ph_2PSe)-6-(Ph_2P)-$C_6H_3SiMe_2H$ (4c). A suspension of 2 (0.55 g, 1.1 mmol) and selenium (85 mg, 1.1 mmol) in anhydrous THF (20 mL) was stirred under argon for 24 h at room temperature. The reaction mixture was filtered through a pad of Celite and the solvent removed by rotary evaporation. Purification by column chromatography with *n*-hexane/$CHCl_3$ (4:1.5) using aluminum oxide as stationary phase afforded **4c** as a white solid (0.53 g, 0.9 mmol, 82 %; Mp. 196 °C).

^{1}H-NMR (200 MHz, $CDCl_3$): δ = 7.94–7.77 (m, 4H), 7.54–6.92 (m, 19H), 5.29–5.07 (m, 1H, $^1J(^{29}Si\text{-}^1H)$ = 196 Hz), 0.41 (t, *J* = 4 Hz, 1H). $^{13}C\{^1H\}$-

Full Paper
doi.org/10.1002/ejic.202000800

NMR (50 MHz, $CDCl_3$): δ = 152.6 (dd, *J* = 51, 17 Hz), 148.1 (apparent t, *J* = 14 Hz), 140.6 (dd, *J* = 78, 17 Hz), 138.4 (d, *J* = 3 Hz), 137.5 (d, *J* = 12 Hz), 134.1, 133.8, 133.1 (d, *J* = 18 Hz), 132.9 (d, *J* = 10 Hz), 132.3, 131.4 (d, *J* = 4 Hz), 128.7, 128.6, 128.5, 128.27, –0.4 (d, *J* = 20.0 Hz). $^{31}P\{^1H\}$-NMR (81 MHz, $CDCl_3$): δ = 39.6 (d, $^4J(^{31}P\text{-}^{31}P)$ = 4 Hz, $^1J(^{31}P–^{77}Se)$ = 729 Hz), –8.9 (d, $^4J(^{31}P\text{-}^{31}P)$ = 4.0 Hz). $^{29}Si\{^1H\}$-NMR (72 MHz, $CDCl_3$): δ = –22.5 (t, $^3J(^{31}P–^{29}Si)$ = 11 Hz). ^{77}Se-NMR: δ = –189.7 (d, $^1J(^{31}P–^{77}Se)$ = 729 Hz). IR (KBr): $\tilde{\nu}$(Si–H) = 2201. MS (ESI^+): 583 $[M - H]^+$.

Synthesis of $[2,6\text{-}(Ph_2PO)_2C_6H_3SiMe_2]^+[Br_3]^-$ (5a·Br_3^-). A solution of **3a** (120 mg, 0.2 mmol) and bromine (64 mg, 0.4 mmol) in THF (10 mL) was stirred for 5 h at room temperature. The solvent was removed to give a red-brownish residue. Recrystallization from dichloromethane afforded red-brownish crystals of **5a**·Br_3^- (172 mg, 0.22 mmol, 99 %; 210 °C dec.).

^{1}H-NMR (200 MHz, $CDCl_3$): δ = 8.55–8.40 (m, 3H), 7.92–7.45 (m, 20H), 0.77 (s, 6H). $^{13}C\{^1H\}$-NMR (91 MHz, $CDCl_3$): δ = 135.6 (d, *J* = 14 Hz), 134.8 (d, *J* = 3 Hz), 132.2 (d, *J* = 12 Hz), 130.0 (d, *J* = 13 Hz), 125.3 (d, *J* = 108 Hz), 4.9. $^{29}Si\{^1H\}$-NMR (72 MHz, $CDCl_3$): δ = –30.9. $^{31}P\{^1H\}$-NMR (81 MHz, $CDCl_3$): δ = 43.6 (s, $^1J(^{13}C\text{-}^{31}P)$ = 108 Hz, $^3J(^{29}Si\text{-}^{31}P)$ = 13 Hz). MS (ESI^+): *m*/*z* = 535.4 $[M]^+$.

Synthesis of $[2,6\text{-}(Ph_2PS)_2C_6H_3SiMe_2]^+[B(C_6F_5)_4]^-$ (5b·$[B(C_6F_5)_4]^-$). A solid mixture of **3b** (57.9 mg, 0.1 mmol) and $Ph_3C[B(C_6F_5)_4]$ (100 mg, 0.1 mmol) were dissolved in C_6D_6 (400 µL). At first two layers formed, which fused into one layer after about 10 h. The crude reaction mixture was assessed by ^{31}P NMR spectroscopy (see Figure 1). Sulfur (6.2 mg, 0.2 mmol) was added and the mixture was kept at room temperature for 5 days (reaction progress was monitored by ^{31}P NMR see ESI for details) then was heated under gentle reflux for 12 h. Crystallization produced few colorless crystals of **5b**·$[B(C_6F_5)_4]^-$ imbedded in a black resin.

$^{29}Si\{^1H\}$-NMR (72 MHz, C_6D_6): δ = –5.7(t, $^3J(^{31}P\text{-}^{29}Si)$ = 4 Hz). $^{31}P\{^1H\}$-NMR (81 MHz, C_6D_6): δ = 50.4. MS (ESI^+): *m*/*z* = 567.3 $[M]^+$.

Synthesis of $[2,6\text{-}(Ph_2PSe)_2C_6H_3SiMe_2]^+[B(C_6F_5)_4]^-$ (5c·$[B(C_6F_5)_4]^-$). A solid mixture of **3c** (57.9 mg, 0.09 mmol) and $[Ph_3C][B(C_6F_5)_4]$ (80.5 mg, 0.09 mmol) were dissolved in C_6D_6 (400 µL). At first two layers formed, which fused into one layer after about 10 h. The crude reaction mixture was assessed by ^{31}P NMR spectroscopy (see Figure 1). Crystallization produced few colorless crystals of **5c**·$[B(C_6F_5)_4]^-$ imbedded in a black resin.

$^{13}C\{^1H\}$-NMR (50 MHz, $CDCl_3$): δ = 153.1 (t, *J* = 24 Hz), 149.12 (d of multiplet, $^1J(^{19}F\text{-}^{13}C)$ = 237 Hz) 140.6 (dd, $^1J(^{31}P\text{-}^{13}C)$ = 79 Hz, $^3J(^{31}P\text{-}^{13}C)$ = 16 Hz), 138.91 (d of multiplet, $^1J(^{19}F\text{-}^{13}C)$ = 247 Hz), 137.16 (d of multiplet, $^1J(^{19}F\text{-}^{13}C)$ = 231.9 Hz), 135.3 (dd, *J* = 12, 2 Hz), 134.3 (s), 132.9 (d, *J* = 11 Hz), 131.1 (t, *J* = 11 Hz), 129.9 (d, *J* = 14 Hz), 125.36 (d, *J* = 78.6 Hz), 1.44 (s). $^{29}Si\{^1H\}$-NMR (72 MHz, $CDCl_3$): δ = –1.1 (s). $^{31}P\{^1H\}$-NMR (81 MHz, $CDCl_3$): δ = 44.7 ppm (s, $^1J(^{77}Se\text{-}^{31}P)$ = 586 Hz, $^3J(^{29}Si\text{-}^{31}P)$ = 78 Hz). ^{77}Se-NMR (69 MHz, $CDCl_3$): δ = –122.3 ppm (d, $^1J(^{77}Se\text{-}^{31}P)$ = 586 Hz). MS (ESI^+): *m*/*z* = 663.1 $[M]^+$.

Synthesis of $[2\text{-}(Ph_2PS)\text{-}6\text{-}(Ph_2PO)C_6H_3SiMe_2]^+[B(C_6F_5)_4]^-$ (7·$[B(C_6F_5)_4]^-$). A solid mixture of **4b** (53.6 mg, 0.1 mmol) and $[Ph_3C][B(C_6F_5)_4]$ (100 mg, 0.1 mmol) were dissolved in C_6D_6 (400 µL). At first two layers formed, which fused into one layer after about 10 h. ^{31}P NMR spectroscopy indicated quantitative formation of **6b·[B(C_6F_5)$_4$]**. The NMR tube was opened to the air for 15 min after which ^{31}P NMR spectroscopy indicated formation of **7**·$[B(C_6F_5)_4]^-$. Addition of *n*-hexane (400 µL) induced crystallization and afforded colorless crystals of **7**·$[B(C_6F_5)_4]^-$ (119 mg, 0.10 mmol, 97 %).

^{1}H-NMR (200 MHz, $CDCl_3$): δ = 8.0–7.5 (m, 23H), 0.9 (6H, s). $^{13}C\{^1H\}$-NMR (200 MHz, $CDCl_3$): δ = 148.29 (d of multiplet, $^1J(^{19}F\text{-}^{13}C)$ = 246 Hz), 138.3 (d of multiplet, $^1J(^{19}F\text{-}^{13}C)$ = 242 Hz), 137.3 (d, *J* = 12 Hz), 136.3 (d, *J* = 2 Hz), 136.6 (d of multiplet, $^1J(^{19}F\text{-}^{13}C)$ = 235 Hz), 133.7 (d, *J* = 2 Hz), 133.4 (d, *J* = 3 Hz), 132.4 (d, *J* = 4 Hz), 132.20 (d, *J* = 3 Hz), 130.4 (d, *J* = 14 Hz), 129.5 (d, *J* = 14 Hz) 128.9, 128.6, 128.4, 128.2, 127.0, 126.3, 123.3, 121.1, 7.7. $^{29}Si\{^1H\}$-NMR (72 MHz, $CDCl_3$): δ = 5.9 (t, $^3J(^{31}P\text{-}^{29}Si)$ = 3 Hz). $^{31}P\{^1H\}$-NMR (81 MHz, $CDCl_3$): δ = 56.7 (s, ^1J ($^{13}C\text{-}^{31}P$) = 12 Hz), 46.8 (s, ^1J ($^{13}C\text{-}^{31}P$) = 11 Hz) ppm. MS (ESI^+): *m*/*z* = 551.3 $[M]^+$.

Synthesis of $[2\text{-}(Ph_2PS)\text{-}6\text{-}[Ph_2P(AuC_6F_5)]C_6H_3SiMe_2]^+[BAr^F]^-$ (8b·$[BAr^F]^-$). NMR monitored experiment. In the glovebox, an NMR tube was charged with **4b** (78 mg, 0.145 mmol) and $[Ph_3C][BAr^F]$ (160 mg, 0.145 mmol). Anhydrous C_6D_6 (1 mL) was added to the solid mixture. The NMR tube was shaken occasionally for the next 3 h then was left standing for additional 12 h. Two layers formed. The dark red bottom layer was assessed by ^{1}H NMR, ^{31}P and ^{29}Si NMR; a complete and clean conversion of **4b** into **6b**·$[BAr^F]^-$ was observed.

$^{31}P\{^1H\}$-NMR (C_6D_6): δ = 60.8 (s), –6.7 (s). $^{29}Si\{^1H\}$ NMR (C_6D_6): 40.0 (d, *J* = 13.3 Hz).

The NMR tube was brought back in the glovebox and to the crude **6b**·$[BAr^F]^-$ was added (tht)AuC_6F_5 (66 mg, 0.146 mmol). The NMR tube was shaken for approximately 5 minutes. The upper layer removed and the bottom layer washed with C_6D_6 (3×0.5 mL). Full conversion of **6b**·$[BAr^F]^-$ and formation of **8b**·$[BAr^F]^-$ was observed by ^{31}P- and ^{29}Si-NMR.

$^{31}P\{^1H\}$-NMR (81 MHz, C_6D_6): δ = 57.6 (d, $^4J(^{31}P\text{-}^{31}P)$ = 1 Hz), 41.9 (apparent quintet, *J* = 8 Hz). $^{29}Si\{^1H\}$-NMR (72 MHz, C_6D_6): δ = 41.2 (d, *J* = 8 Hz).

Isolation of 8b·$[BAr^F]^-$. In the glovebox, a vial was charged with **4b** (116 mg, 0.216 mmol) and trityl tetrakis[3,5-bis(trifluoromethyl)phenyl]borate (239 mg, 0.216 mmol). Anhydrous fluorobenzene (3 mL) was added. The mixture was stirred for 20 min then to the crude **6b**·$[BAr^F]^-$ was added (tht)AuC_6F_5 (98 mg, 0.216 mmol) and stirring was continued for 10 additional minutes. The red solution was layered with *n*-hexane (approx. 7 mL) and the vial left standing for a week. After this time a red oily layer separated at the bottom of the vial. The vial was placed in a freezer at –30 °C for several days causing the precipitation of a crystalline solid. The solution was removed and the solid washed with *n*-hexane (3×5 mL) then dried. Compound **8b**·$[BAr^F]^-$ was obtained as a tan solid (315 mg, 0.179 mmol, 83 %; Mp. 153–155 °C dec.). Crystals suitable for X-ray diffraction were obtained by diffusion of *n*-hexane vapors into a concentrated solution of **8b**·$[BAr^F]^-$ in CH_2Cl_2 (approx. 0.3 mL).

^{1}H-NMR (200 MHz, C_6D_6): δ = 8.30 (s, 8H, BAr^F), 7.55 (s, 4H, BAr^F) 7.30–6.67 (m, 23H), 0.62 (s, 6H). $^{13}C\{^1H\}$-NMR (50 MHz, C_6D_6): δ = 162.8 (q, $^1J(^{13}C–^{11}B)$ = 49 Hz, sept, $^1J(^{13}C–^{10}B)$ = 17 Hz), 149.3 (dd of multiplet, $^1J(^{13}C–^{19}F)$ = 224, $^2J(^{13}C–^{19}F)$ = 24 Hz), 148.3 (t, *J* = 27 Hz), 140.2 (d, $^1J(^{13}C–^{19}F)$ = 248 Hz), 140.2–127.1 (multiple resonances overlapped), 122.5, 121.9, 120.2, 118.1, 117.1, 5.4. $^{31}P\{^1H\}$-NMR (81 MHz, C_6D_6): δ = 57.6 (d, $^4J(^{31}P\text{-}^{31}P)$ = 1 Hz), 41.9 (apparent quintet, *J* = 8 Hz). ^{19}F-NMR (188 MHz, C_6D_6): δ = –63.4 (s, 24F, BAr^F), –116.8 to –117.4 (m, 2F), –158.1 (t, *J* = 20 Hz, 1F), –162.5 to –163.2 (m, 2F). $^{29}Si\{^1H\}$-NMR (72, MHz, C_6D_6): δ = 41.2 (d, *J* = 8 Hz).

Synthesis of $[2\text{-}(Ph_2PSe)\text{-}6\text{-}[Ph_2P(AuC_6F_5)]C_6H_3SiMe_2]^+[BAr^F]^-$ (8c·$[BAr^F]^-$). NMR monitored experiment. In the glovebox, an NMR tube was charged with **4c** (85 mg, 0.145 mmol) and $[Ph_3C][BAr^F]$ (160 mg, 0.145 mmol). Anhydrous C_6D_6 (1 mL) was added to the solid mixture. The NMR tube was shaken occasionally for the next 3 h then was left standing for additional 9 h. Two layers formed. The dark yellow bottom layer was assessed by ^{31}P and ^{29}Si

NMR; a complete conversion of **4c** was observed. The formation of **6c**·$[BAr^F]^-$, **5c**·$[BAr^F]^-$, and of an unidentified side-product in a 1:0.25:0.11 molar ratio was indicated by ^{31}P-NMR.

^{31}P{^{1}H}-NMR (81, MHz, C_6D_6): δ = 53.7 (s, $^1J(^{31}P–^{77}Se)$ = 469 Hz, P=Se of **6c**·$[BAr^F]^-$), 44.7 (s, $^1J(^{31}P–^{77}Se)$ = 470 Hz, P=Se of **5c**·$[BAr^F]^-$), –4.2 (s, side-product), –7.6 (s, P of **6c**·$[BAr^F]^-$). **^{29}Si{^{1}H}-NMR (72 MHz, C_6D_6)**: δ = 38.5 (d, J = 13.6 Hz, $^1J(^{29}Si–^{77}Se)$ = 85 Hz, **6c**·$[BAr^F]^-$). **^{77}Se-NMR (69, MHz, C_6D_6)**: δ = –147.9 (d, $^1J(^{31}P–^{77}Se)$ = 470 Hz).

The NMR tube was brought in the glovebox and to the crude mixture containing **6c**·$[BAr^F]^-$ was added (tht)AuC_6F_5 (65 mg, 0.145 mmol). The NMR tube was shaken for approximately 5 minutes. The upper layer removed and the bottom layer washed with C_6D_6 (6×0.35 mL). Complete conversion of **6c**·$[BAr^F]^-$ and formation of the target product **8c**·$[BAr^F]^-$ was indicated by ^{31}P and ^{29}Si NMR. Compound **5c**·$[BAr^F]^-$ was present in approximately the same amount with respect to **8c**·$[BAr^F]^-$. The solvent was than evaporated in the glovebox and the remaining oil dissolved in fluorobenzene. Crystals suitable for X-ray diffraction were obtained by diffusion of *n*-hexane vapors into a concentrated solution of **8b**·$[BAr^F]^-$ in PhF.

^{31}P{^{1}H}-NMR (81 MHz, C_6D_6): δ = 50.7 (d, $^4J(^{31}P–^{31}P)$ = 2 Hz, $^1J(^{31}P–^{77}Se)$ = 452 Hz), 41.9 (apparent quintet, J = 8 Hz). ^{29}Si{^{1}H} NMR (72 MHz, C_6D_6): δ = 40.3 (d, J = 8 Hz). ^{77}Se-NMR (69 MHz, C_6D_6): δ = –104.8 (d, $^1J(^{31}P–^{77}Se)$ = 447 Hz).

Isolation of 8c·$[BAr^F]^-$. In the glovebox, a vial was charged with **4c** (130 mg, 0.223 mmol) and trityl tetrakis[3,5-bis(trifluoromethyl)-phenyl]borate (247 mg, 0.223 mmol). Anhydrous fluorobenzene (3 mL) was added. The mixture was stirred for 40 min. The color of the solution changed from brown-green to red. To the crude **6c**·$[BAr^F]^-$ was added (tht)AuC_6F_5 (101 mg, 0.223 mmol) and stirring was continued for 10 additional minutes. The red solution was layered with *n*-hexane (approx. 7 mL) and the vial left standing for a week. The yellow crystals obtained were separated from the solution and then washed with *n*-hexane (3×5 mL) and dried. Compound 8c·$[BAr^F]^-$ was obtained as a yellow crystalline solid (380 mg, 0.21 mmol, 94 %; Mp. darkens at 148–155 °C; black melt at 165–167 °C dec.). The product contained 3 % molar **5c**·$[BAr^F]^-$.

^{1}H (200 MHz, C_6D_6): δ = 8.30 (s, 8H, BAr^F), 7.55(s, 4H, BAr^F), 7.33–6.65 (m, 23H), 0.69 (s, 6H). ^{13}C{^{1}H}-NMR (50 MHz, C_6D_6): δ = 162.8 (q, $^1J(^{13}C–^{11}B)$ = 49 Hz, sept, $^1J(^{13}C–^{10}B)$ = 17 Hz), 149.3 (dd of multiplet, $^1J(^{13}C–^{19}F)$ = 226, $^2J(^{13}C–^{19}F)$ = 26 Hz), 149.3 (t, J = 27 Hz), 140.9, 140.7, 140.4,140.2 (d of multiplet, $^1J(^{13}C–^{19}F)$ = 248 Hz), 139.9–127.2 (multiple resonances overlapped), 122.5, 121.8, 120.3, 118.1, 117.1, 6.2. ^{31}P{^{1}H}-NMR (81 MHz, C_6D_6): δ = 50.7 (d, $^4J(^{31}P–^{31}P)$ = 2 Hz, $^1J(^{31}P–^{77}Se)$ = 452 Hz), 41.9 (apparent quintet, J = 8 Hz). ^{19}F-NMR (188 MHz, C_6D_6): δ = –63.4 (s, 24F, BAr^F), –116.7 to –117.2 (m, 2F), –158.2 (t, J = 20 Hz, 1F), –162.5 to –163.1 (m). ^{29}Si{^{1}H} NMR (72 MHz, C_6D_6): δ = 40.3 (d, J = 8 Hz, $^1J(^{29}Si–^{77}Se)$ = 82 Hz). ^{77}Se-NMR (69 MHz, C_6D_6): δ = –104.8 (d, $^1J(^{31}P–^{77}Se)$ = 447 Hz).

Crystal structure determination. The X-ray data collection was carried out using Mo-K_α radiation on a Siemens P4 diffractometer (**2**, **3a**-**3c**, **4b**, **5a**), on Stoe IPDS I diffractometer (**5c**) and on Bruker Venture diffractometer (**7**, **8b**, **8c**, $Ph_3COOCPh_3$) respectively. Single-crystal structures were solved and refined on F^2 with *SHELXL*-2013[41] (except of **8b**–**c**, for which *SHELXL*-2014[41] was used) including anisotropic displacement parameters for all non-hydrogen atoms. In structure **7**, a group of atoms (S2, O1, P1, P2, C1 C2) were refined as disordered over two sets of sites with occupancy factors equal to 0.905(1):0.095(1). Additionally, similarity restraints of the atomic displacements parameters of all disordered atoms were used in the refinement of **7**. In all structures (C)–H-atoms were located in calculated positions and refined isotropically using a rigid body model.

In **2**, **3a–c** and **4b**, the H atoms attached to Si were found on the difference map and their positional parameters were refined with U_{iso}= –1.5 U_{eq}(Si) (except for structures **3c** and **4b,** where this H-atom was constrained to Si). In structure (**3a**) a solvent water molecule was refined with hydrogen atoms constrained to oxygen atom. Further details of crystal data and measurement conditions are given in Tables S1–S3 in the Supporting Information (SI). The *ORTEP* drawings were made using *Mercury*.[42] Deposition Numbers 1024517 (**2**), 1024518 (**3a**), 1024519 (**3b**), 1024520 (**3c**), 1024521 (**4b**), 1024506 (**5a**), 1024507 (**5c**), 1024508 (**7**), 1424430 (**8b**), 1424431 (**8c**) and 1024509 ($Ph_3COOCPh_3$). Copies of the data can be obtained free of charge on application to The Director, CCDC, 12 Union Road, Cambridge CB2 1 contain the supplementary crystallographic data for this paper. These data are provided free of charge by the joint Cambridge Crystallographic Data Centre and Fachinformationszentrum Karlsruhe Access Structures service www.ccdc.cam.ac.uk/structures.

Computational chemistry. On the basis of experimental X-ray single-crystal coordinates of the precursors (**2**, **3a–c**) and the E,C,E′-pincer supported silyl cations (**5a**, E = O; **5c**, E = Se), a full geometry optimization of the gas-phase molecules was performed with the functional B3PW91[43] and the 6-311++G(2df,p)[44] basis-set using the program package *Gaussian09*.[45] Since the X-ray structure of the S,C,S′-pincer cation (**5b**) was not determined, its gas-phase geometry was predicted and optimized using starting geometry of (**5a**) with S atoms instead of O atoms. The single-point calculations of the E,C,Au-pincer supported silyl cations (**8b**, E = S; **8c**, E = Se) were performed at the B3PW91 level of theory using the effective core potential for Au[46] with the associated triple-ζ basis-set[46] and the 6-311++G(2df,p)[44] basis-set for all other atoms.

Complete topological analysis of the electron density was performed according to Bader's quantum theory of atoms in molecules (QTAIM) using *AIM2000*[47] and *AIMAll*.[48] The ELI-D bond properties were calculated from the *Gaussian* checkpoint file using the program *DGrid*-4.6[49] with the grid step size 0.06 au.

Acknowledgments

The Deutsche Forschungsgemeinschaft (DFG) is gratefully acknowledged for financial support. L. C. acknowledges the Deutsche Akademischer Austauschdienst (DAAD) for a two-month fellowship. O. M. acknowledges the financial support of the National University Research Council (CNCS) of Romania - project PN-II-ID-PCCE-2011-2–0050 (9/2012). We are grateful to Umicore (Hanau, Germany) for a donation of precious metals.

Keywords: Pincer ligands · Intramolecular coordination · Silyl cations · Chalcogenes · Silicon

[1] a) J. B. Lambert, L. Kania, S. Zhang, *Chem. Rev.* **1995**, *95*, 1191–1201; b) C, A. Reed, *Acc. Chem. Res.* **1998**, *31*, 325–332; c) J. B. Lambert, Y. Zhao, S. M. Zhang, *J. Phys. Org. Chem.* **2001**, *14*, 370–379; d) T. Müller, *Struct. Bonding (Berlin)* **2014**, *155*, 107–162; e) V. Y. Lee, A. Sekiguchi in *Organosilicon Compounds*, vol. 1 (Ed.: V. Y. Lee), Academic Press, San Diego, **2017**, p. 197–230.

[2] K.-C. Kim, C. A. Reed, D. W. Elliott, L. J. Mueller, F. Tham, L. Lin, J. B. Lambert, *Science* **2002**, *297*, 825–827.

[3] A. Schäfer, M. Reißmann, S. Jung, A. Schäfer, W. Saak, E. Brendler, T. Müller, *Organometallics* **2013**, *32*, 4713–4722.

[4] T. Küppers, E. Bernhardt, R. Eujen, H. Willner, C. W. Lehmann, *Angew. Chem. Int. Ed.* **2007**, *46*, 6346–6349; *Angew. Chem.* **2007**, *119*, 6462.
[5] M. Kessler, C. Knapp, V. Sagawe, H. Scherer, R. Uzun, *Inorg. Chem.* **2010**, *49*, 5223–5230.
[6] C. Douvris, C. M. Nagaraja, C.-H. Chen, B. M. Foxman, O. V. Ozerov, *J. Am. Chem. Soc.* **2010**, *132*, 4946–4953.
[7] Q. Wu, E. Irran, R. Müller, M. Kaupp, H. F. T. Klare, M. Oestreich, *Science* **2019**, *365*, 168–172.
[8] M. F. Ibad, P. Langer, A. Schulz, A. Villinger, *J. Am. Chem. Soc.* **2011**, *133*, 21016–21027.
[9] a) S. Duttwyler, Q.-Q. Do, A. Linden, K. K. Baldridge, J. S. Siegel, *Angew. Chem. Int. Ed.* **2008**, *47*, 1719–1722; *Angew. Chem.* **2008**, *120*, 1743; b) P. Romanato, S. Duttwyler, A. Linden, K. K. Baldridge, J. S. Siegel, *J. Am. Chem. Soc.* **2010**, *132*, 7828–7829; c) P. Romanato, S. Duttwyler, A. Linden, K. K. Baldridge, J. S. Siegel, *J. Am. Chem. Soc.* **2011**, *133*, 11844–11846.
[10] a) K. Müther, R. Fröhlich, C. Mück-Lichtenfeld, S. Grimme, M. Oestreich, *J. Am. Chem. Soc.* **2011**, *133*, 12442–12444; b) A. Simonneau, T. Biberger, M. Oestreich, *Organometallics* **2015**, *34*, 3927–3929.
[11] a) T. Müller, *Angew. Chem. Int. Ed.* **2001**, *40*, 3033–3036; *Angew. Chem.* **2001**, *113*, 3123; b) S. P. Hoffmann, T. Kato, F. S. Tham, C. A. Reed, *Chem. Commun.* **2006**, 767–769; c) Y. A. Khalimon, Z. H. Lin, R. Simionescu, S. F. Vyboishchikov, G. I. Nikonov, *Angew. Chem. Int. Ed.* **2007**, *46*, 4530–4533; *Angew. Chem.* **2007**, *119*, 4614; d) M. Nava, C. A. Reed, *Organometallics* **2011**, *30*, 4798–4800; e) S. J. Connelly, W. Kaminsky, D. M. Heinekey, *Organometallics* **2013**, *32*, 7478–7481.
[12] a) A. D. Dilman, S. L. Ioffe, *Chem. Rev.* **2003**, *103*, 733–772; b) H. F. T. Klare, M. Oestreich, *Dalton Trans.* **2010**, *39*, 9176–9184.
[13] a) R. Panisch, M. Bolte, T. Müller, *J. Am. Chem. Soc.* **2006**, *128*, 9676–9682; b) O. Allemann, K. K. Baldridge, J. S. Siegel, *Org. Chem. Front.* **2015**, *2*, 1018–1021.
[14] a) K. Hara, R. Akiyama, M. Sawamura, *Org. Lett.* **2005**, *7*, 5621–5623; b) H. F. T. Klare, K. Bergander, M. Oestreich, *Angew. Chem. Int. Ed.* **2009**, *48*, 9077–9079; *Angew. Chem.* **2009**, *121*, 9241; c) A. R. Nödling, K. Müther, V. H. G. Rohde, G. Hilt, M. Oestreich, *Organometallics* **2014**, *33*, 302–308; d) V. H. G. Rohde, P. Pommerening, H. F. T. Klare, M. Oestreich, *Organometallics* **2014**, *33*, 3618–3628.
[15] a) A. Schäfer, M. Reißmann, A. Schäfer, W. Saak, D. Haase, T. Müller, *Angew. Chem. Int. Ed.* **2011**, *50*, 12636–12638; *Angew. Chem.* **2011**, *123*, 12845; b) M. Reißmann, A. Schäfer, S. Jung, T. Müller, *Organometallics* **2013**, *32*, 6736–6744.
[16] a) C. Chuit, R. J. P. Corriu, A. Mehdi, C. Reye, *Angew. Chem. Int. Ed. Engl.* **1993**, *32*, 1311–1313; *Angew. Chem.* **1993**, *105*, 1372–1375; b) F. Carré, C. Chuit, R. J. P. Corriu, A. Mehdi, C. Reye, *Angew. Chem. Int. Ed. Engl.* **1994**, *33*, 1097–1099; *Angew. Chem.* **1994**, *106*, 1152–1154; c) M. Chauhan, C. Chuit, R. J. P. Corriu, A. Mehdi, C. Reye, *Organometallics* **1996**, *15*, 4326–4333; d) A. Bockholt, P. Jutzi, A. Mix, B. Neumann, A. Stammler, H.-G. Stammler, *Z. Anorg. Allg. Chem.* **2009**, *635*, 1326–1334.
[17] a) K. Peveling, M. Schürmann, R. Ludwig, K. Jurkschat, *Organometallics* **2001**, *20*, 4654–4663; b) K. Peveling, M. Henn, C. Löw, M. Mehring, M. Schürmann, B. Costisella, K. Jurkschat, *Organometallics* **2004**, *23*, 1501–1508; c) K. Dannappel, M. Schürmann, B. Costisella, K. Jurkschat, *Organometallics* **2005**, *24*, 1031–1034; d) K. Peveling, K. Dannappel, M. Schürmann, B. Costisella, K. Jurkschat, *Organometallics* **2006**, *25*, 368–374.
[18] a) D. B. Chesnut, A. Savin, *J. Am. Chem. Soc.* **1999**, *121*, 2335–2336; b) R. Kather, T. Svoboda, M. Wehrhahn, E. Rychagova, E. Lork, L. Dostál, S. Ketkov, J. Beckmann, *Chem. Commun.* **2015**, *51*, 5932–5935.
[19] a) D. Himmel, I. Krossing, A. Schnepf, *Angew. Chem. Int. Ed.* **2014**, *53*, 370–374; *Angew. Chem.* **2014**, *126*, 378; b) G. Frenking, *Angew. Chem. Int. Ed.* **2014**, *53*, 6040–6046; *Angew. Chem.* **2014**, *126*, 6152; c) D. Himmel, I. Krossing, A. Schnepf, *Angew. Chem. Int. Ed.* **2014**, *53*, 6047–6048; *Angew. Chem.* **2014**, *126*, 6159; d) S. Mebs, J. Beckmann, *J. Phys. Chem. A* **2017**, *121*, 7717–7725; e) A. Nandi, S. Kozuch, *Chem. Eur. J.* **2020**, *26*, 759–772.
[20] a) R. J. Gillespie, S. A. Johnson, *Inorg. Chem.* **1997**, *36*, 3031–3039; b) N. Kocher, J. Henn, B. Gostevskii, D. Kost, I. Kalikhman, B. Engels, D. Stalke, *J. Am. Chem. Soc.* **2004**, *126*, 5563–5568; c) S. Grabowsky, M. F. Hesse, C. Paulmann, P. Luger, J. Beckmann, *Inorg. Chem.* **2009**, *48*, 4384–4394; d) M. Fugel, M. F. Hesse, R. Pal, J. Beckmann, D. Jayatilaka, M. J. Turner, A. Karton, P. Bultinck, G. S. Chandler, S. Grabowsky, *Chem. Eur. J.* **2018**, *24*, 15275–15286.
[21] J. Fischer, M. Schürmann, M. Mehring, U. Zachwieja, K. Jurkschat, *Organometallics* **2006**, *25*, 2886–2893.
[22] a) M. Olaru, E. Ryhagova, S. Ketkov, Y. Shykarenko, S. Yakunin, M. V. Kovalenko, A. Yablonskiy, B. Andreev, F. Kleemiss, J. Beckmann, M. Vogt, *J. Am. Chem. Soc.* **2020**, *142*, 373–381; b) M. Olaru, J. F. Kögel, R. Aoki, R. Sakamoto, H. Nishihara, E. Lork, S. Mebs, M. Vogt, J. Beckmann, *Chem. Eur. J.* **2020**, *26*, 275–284.
[23] R. F. W. Bader, *Atoms in Molecules. A Quantum Theory*, Clarendon Press, Oxford, **1994**.
[24] a) M. Kohout, *Int. J. Quantum Chem.* **2004**, *97*, 651–658; b) M. Kohout, F. R. Wagner, Y. Grin, *Theor. Chem. Acc.* **2008**, *119*, 413–420.
[25] C. Tamborski, E. J. Soloski, *J. Org. Chem.* **1966**, *31*, 746–749.
[26] B. Bennetau, F. Rajarison, J. Dunoguès, *Tetrahedron* **1993**, *49*, 10843–10854.
[27] J. Beckmann, M. Hesse, *Z. Anorg. Allg. Chem.* **2007**, *633*, 1233–1238.
[28] a) P. Politzer, J. S. Murray, P. Lane, M. C. Concha, *Int. J. Quantum Chem.* **2009**, *109*, 3773–3780; b) K. J. Donald, B. K. Wittmaack, C. Crigger, *J. Phys. Chem. A* **2010**, *114*, 7213–7222; c) K. J. Donald, M. Tawfik, *J. Phys. Chem. A* **2013**, *117*, 14176–14183; d) S. J. Grabowski, *Phys. Chem. Chem. Phys.* **2014**, *16*, 1824–1834.
[29] a) A. Bondi, *J. Phys. Chem.* **1964**, *68*, 441–451; b) S. Alvarez, *Dalton Trans.* **2013**, *42*, 8617–8636.
[30] T. Steiner, *Angew. Chem. Int. Ed.* **2002**, *41*, 48–76; *Angew. Chem.* **2002**, *114*, 50.
[31] H. Schmidbaur, H. G. Raubenheimer, L. Dobrzańska, *Chem. Soc. Rev.* **2014**, *43*, 345–380.
[32] C. B. Hübschle, P. Luger, *J. Appl. Crystallogr.* **2006**, *39*, 901–904.
[33] E. Espinosa, I. Alkorta, J. Elguero, E. Molins, *J. Chem. Phys.* **2002**, *117*, 5529–5542.
[34] a) S. Raub, G. Jansen, *Theor. Chem. Acc.* **2001**, *106*, 223–232; b) I. Vidal, S. Melchor, J. A. Dobado, *J. Phys. Chem. A* **2005**, *109*, 7500–7508.
[35] a) R. F. W. Bader, M. E. Stephens, *J. Am. Chem. Soc.* **1975**, *97*, 7391–7399; b) X. Fradera, M. A. Austen, R. F. W. Bader, *J. Phys. Chem. A* **1999**, *103*, 304–314.
[36] a) N. Kocher, C. Selinka, D. Leusser, D. Kost, I. Kalikhman, D. Stalke, *Z. Anorg. Allg. Chem.* **2004**, *630*, 1777–1793; b) H. Ott, C. Däschlein, D. Leusser, D. Schildbach, T. Seibel, D. Stalke, C. Strohmann, *J. Am. Chem. Soc.* **2008**, *130*, 11901–11911; c) P. Luger, M. Weber, C. Hübschle, R. Tacke, *Org. Biomol. Chem.* **2013**, *11*, 2348–2354.
[37] a) J. Beckmann, E. Hupf, E. Lork, S. Mebs, *Inorg. Chem.* **2013**, *52*, 11881–11888; b) E. Hupf, E. Lork, S. Mebs, L. Chęcińska, J. Beckmann, *Organometallics* **2014**, *33*, 7247–7259; c) S. Furan, E. Hupf, E. Lork, S. Mebs, J. Beckmann, *Eur. J. Inorg. Chem.* **2017**, 3302–3311.
[38] a) R. Janicki, P. Starynowicz, *Acta Crystallogr., Sect. B: Struct. Sci.* **2010**, *66*, 559–567; b) A. Mermer, P. Starynowicz, *Acta Crystallogr., Sect. B: Struct. Sci.* **2011**, *67*, 399–408; c) A. Mermer, P. Starynowicz, *Acta Crystallogr., Sect. B* **2012**, *68*, 625–635; d) M. Małecka, S. Mondal, S. van Smaalen, C. Paulmann, *Acta Crystallogr., Sect. B* **2013**, *69*, 621–628.
[39] a) N. A. Yakelis, R. G. Bergman, *Organometallics* **2005**, *24*, 3579–3581; b) M. Brookhart, B. Grant, A. F. Volpe Jr., *Organometallics* **1992**, *11*, 3920–3922; c) S. R. Bahr, P. Boudjouk, *J. Org. Chem.* **1992**, *57*, 5545–5547.
[40] T. Lauterbach, M. Livendahl, A. Rosellon, P. Espinet, A. M. Echavarren, *Org. Lett.* **2010**, *12*, 3006–3009.
[41] G. M. Sheldrick, *Acta Crystallogr., Sect. C.* **2015**, *71*, 3–8.
[42] C. F. Macrae, I. J. Bruno, J. A. Chisholm, P. R. Edgington, P. McCabe, E. Pidcock, L. Rodriguez-Monge, R. Taylor, J. van de Streek, P. A. Wood, *J. Appl. Crystallogr.* **2008**, *41*, 466–470.
[43] a) J. P. Perdew, J. A. Chevary, S. H. Vosko, K. A. Jackson, M. R. Pederson, D. J. Singh, C. Fiolhais, *Phys. Rev. B* **1992**, *46*, 6671–6687; b) A. D. Becke, *J. Chem. Phys.* **1993**, *98*, 5648–5652.
[44] a) K. A. Peterson, D. Figgen, E. Goll, H. Stoll, M. Dolg, *J. Chem. Phys.* **2003**, *119*, 11113–11123; b) B. Metz, H. Stoll, M. Dolg, *J. Chem. Phys.* **2000**, *113*, 2563–2569; c) K. A. Peterson, *J. Chem. Phys.* **2003**, *119*, 11099–11112.
[45] M. J. Frisch, G. W. Trucks, H. B. Schlegel, G. E. Scuseria, M. A. Robb, J. R. Cheeseman, G. Scalmani, V. Barone, B. Mennucci, G. A. Petersson, H. Nakatsuji, M. Caricato, X. Li, H. P. Hratchian, A. F. Izmaylov, J. Bloino, G. Zheng, J. L. Sonnenberg, M. Hada, M. Ehara, K. Toyota, R. Fukuda, J. Hasegawa, M. Ishida, T. Nakajima, Y. Honda, O. Kitao, H. Nakai, T. Vreven, J. A. Montgomery Jr., J. E. Peralta, F. Ogliaro, M. Bearpark, J. J. Heyd, E. Brothers, K. N. Kudin, V. N. Staroverov, R. Kobayashi, J. Normand, K. Raghava-

chari, A. Rendell, J. C. Burant, S. S. Iyengar, J. Tomasi, M. Cossi, N. Rega, J. M. Millam, M. Klene, J. E. Knox, J. B. Cross, V. Bakken, C. Adamo, J. Jaramillo, R. Gomperts, R. E. Stratmann, O. Yazyev, A. J. Austin, R. Cammi, C. Pomelli, J. W. Ochterski, R. L. Martin, K. Morokuma, V. G. Zakrzewski, G. A. Voth, P. Salvador, J. J. Dannenberg, S. Dapprich, A. D. Daniels, Ö. Farkas, J. B. Foresman, J. V. Ortiz, J. Cioslowski, D. J. Fox, *Gaussian 09, Revision B.01*, Gaussian, Inc., Wallingford CT, **2010**.

[46] a) D. Figgen, G. Rauhut, M. Dolg, H. Stoll, *Chem. Phys.* **2005**, *311*, 227–244; b) K. A. Peterson, C. Puzzarini, *Theor. Chem. Acc.* **2005**, *114*, 283–296.

[47] F. Biegler-König, J. Schönbohm, D. Bayles, *J. Comput. Chem.* **2001**, *22*, 545–559.

[48] T. A. Keith, *AIMall* (Version 14.11.23, Professional), T. K. Gristmill Software, Overland Park, KS, USA, **2009** (http://aim.tkgristmill.com).

[49] M. Kohout, *DGRID 4.6*, Radebeul, **2011**.

Received: August 25, 2020